


A nitroalkene derivative of salicylate, SANA, induces creatine-dependent thermogenesis and promotes weight loss

Received: 23 June 2023

Accepted: 7 May 2025

Published online: 17 June 2025

 Check for updates

A list of authors and their affiliations appears at the end of the paper

The emergence of glucagon-like peptide-1 agonists represents a notable advancement in the pharmacological treatment of obesity, yet complementary approaches are essential. Through phenotypic drug discovery, we developed promising nitroalkene-containing small molecules for obesity-related metabolic dysfunctions. Here, we present SANA, a nitroalkene derivative of salicylate, demonstrating notable efficacy in preclinical models of diet-induced obesity. SANA reduces liver steatosis and insulin resistance by enhancing mitochondrial respiration and increasing creatine-dependent energy expenditure in adipose tissue, functioning effectively in thermoneutral conditions and independently of uncoupling protein 1 and AMPK activity. Finally, we conducted a randomized, double-blind, placebo-controlled phase 1A/B clinical trial, which consisted of two parts, each with four arms: (A) single ascending doses (200–800 mg) in healthy lean volunteers; (B) multiple ascending doses (200–400 mg per day for 15 days) in healthy volunteers with overweight or obesity. The primary endpoint assessed safety and tolerability. Secondary and exploratory endpoints included pharmacokinetics, tolerability, body weight and metabolic markers. SANA shows good safety and tolerability, and demonstrates beneficial effects on body weight and glucose management within 2 weeks of treatment. Overall, SANA appears to be a first-in-class activator of creatine-dependent energy expenditure and thermogenesis, highlighting its potential as a therapeutic candidate for ‘diabesity’. Australian New Zealand Clinical Trials Registry registration: [ACTRN12622001519741](https://www.anzctr.org.au/Trial/Registration/TrialRegistration.aspx?ACTRN12622001519741).

Obesity and its associated comorbidities, including type II diabetes and cardiovascular disease¹, are a global epidemic, making them substantial drivers of healthcare burdens worldwide. Although obesity is preventable through the adoption of healthy nutrition and lifestyle changes, once the obesity phenotype is established, it becomes difficult to reverse through behavioural changes alone. The recent emergence of glucagon-like peptide-1 (GLP-1) agonists, such as semaglutide, has shown that pharmacological treatment for obesity and its related

comorbidities is now a realistic possibility². However, alternative or complementary approaches to GLP-1-based therapies may help improve long-term outcomes and minimize side effects.

Among the promising molecules for treating metabolic diseases are nitrated unsaturated fatty acids³. These compounds have demonstrated a range of beneficial properties, including positive metabolic effects in preclinical models of obesity^{3–6}, due to their pleiotropic effects. The main pharmacological action of nitro fatty acids stems

✉ e-mail: chini.eduardo@mayo.edu; batthyany@pasteur.edu.uy; escande@pasteur.edu.uy

from their reactive nitroalkene group, which affects several signalling pathways³. Recently, we demonstrated that this nitroalkene group can be transferred to other molecular scaffolds with known pharmacological effects that differ structurally from fatty acids^{7–9}. By repositioning the nitroalkene group onto these scaffolds, we established three key findings: (1) The beneficial signalling properties of the nitroalkene group are preserved in the designed molecules; (2) the scaffold can be used to enhance the pharmacological properties of the nitroalkene group; (3) in some cases, emergent properties arise that could not have been predicted^{7–10}.

Building on these concepts, we developed several nitroalkene-containing small molecules. Using phenotypic drug discovery, we screened these molecules for activity in obesity and related diseases. In the founding generation of molecules, based on a vitamin E scaffold designed for the treatment of atherosclerosis and obesity-induced inflammation, we observed improvements in systemic inflammation, glucose intolerance and atherosclerosis during obesity^{8–10}.

In this work, we show an unprecedented metabolic effect of a nitroalkene-based small molecule, SANA (5-(2-nitroethenyl)salicylic acid), using the ancient drug salicylate as a scaffold. Salicylate, the precursor of aspirin, was used for more than a century to diminish inflammation and relieve pain. It inhibits nuclear factor- κ B signalling and inflammation¹¹. When administered at elevated doses (2–5 g per kg per day), it activates AMPK and improves metabolic dysfunction in obese mice, including modest effects in weight gain^{12–15}. Indeed, salicylate was tested in clinical trials for diabetes, revealing improvement in basal glycaemia, glycosylated haemoglobin and C-reactive protein^{16–18}.

Our data demonstrate that SANA promotes weight loss and protects against diet-induced obesity (DIO), insulin resistance, hypertriglyceridaemia and liver steatosis in rodent preclinical models. Notably, these effects are markedly greater than those previously described for salicylate^{12–14}. Mechanistically, we found that SANA stimulates non-shivering thermogenesis in both brown and white adipose tissue, an unexpected property of this molecule. The effect of SANA was independent of uncoupling protein 1 (UCP1) and AMPK activation and was lost after creatine depletion. Furthermore, *Ckmt1* (encoding ubiquitous mitochondrial creatine kinase) knockout (KO) mice demonstrated impaired thermoregulation after SANA treatment, which was rescued by thermoneutral housing. Importantly, the safety, tolerability, pharmacokinetics and pharmacodynamics of SANA (referred to as MVD1 for clinical development) following both single-dose and multiple-dose administrations were evaluated in a phase 1A/B, first-in-human, randomized, double-blind, placebo-controlled clinical trial. Up to 400 mg a day, SANA demonstrated an overall favourable safety and tolerability profile. In individuals treated with the highest dose of SANA for 15 days, we observed an improvement in homeostatic model assessment for insulin resistance (HOMA-IR) and weight loss, coupled with a favorable safety profile. Taken together, we propose that SANA is not just an improved version of salicylate but a molecule

with unexpected properties, such as its effects in energy homeostasis, and appears to be potentially a viable therapeutic strategy for treating obesity and metabolic syndrome.

Results

SANA prevents DIO

The salicylate-based nitroalkene, SANA, was obtained by a one-step synthetic route with ~93% yield (Extended Data Fig. 1a). SANA showed similar biochemical (that is, Michael addition reactions with low-molecular-weight thiol-containing compounds (Extended Data Fig. 1a) and signalling properties to other nitroalkene compounds in vitro and in vivo (Extended Data Fig. 1b–j). Pharmacokinetic analysis in mice showed maximum plasma concentration (Tmax) of SANA 0.5 h after oral administration (p.o., 400 mg per kg body weight), with a maximum observed plasma concentration (Cmax) of 4850 ng ml⁻¹. SANA was no longer detectable in plasma after 24 h (Extended Data Fig. 2a). Chronic administration of SANA (400 mg per kg per day) to normal mice for 8 weeks showed no signs of renal or liver toxicity (Extended Data Fig. 2b–f). Biodistribution analysis performed by administration of ¹¹C-SANA followed by positron emission tomography and a magnetic resonance imaging (MRI) scan revealed that SANA followed an enterohepatic circuit, being excreted mainly through the kidneys and intestine (Extended Data Fig. 2g–i). Importantly, SANA was also detectable in several tissues including inguinal white adipose tissue (iWAT; Extended Data Fig. 2j).

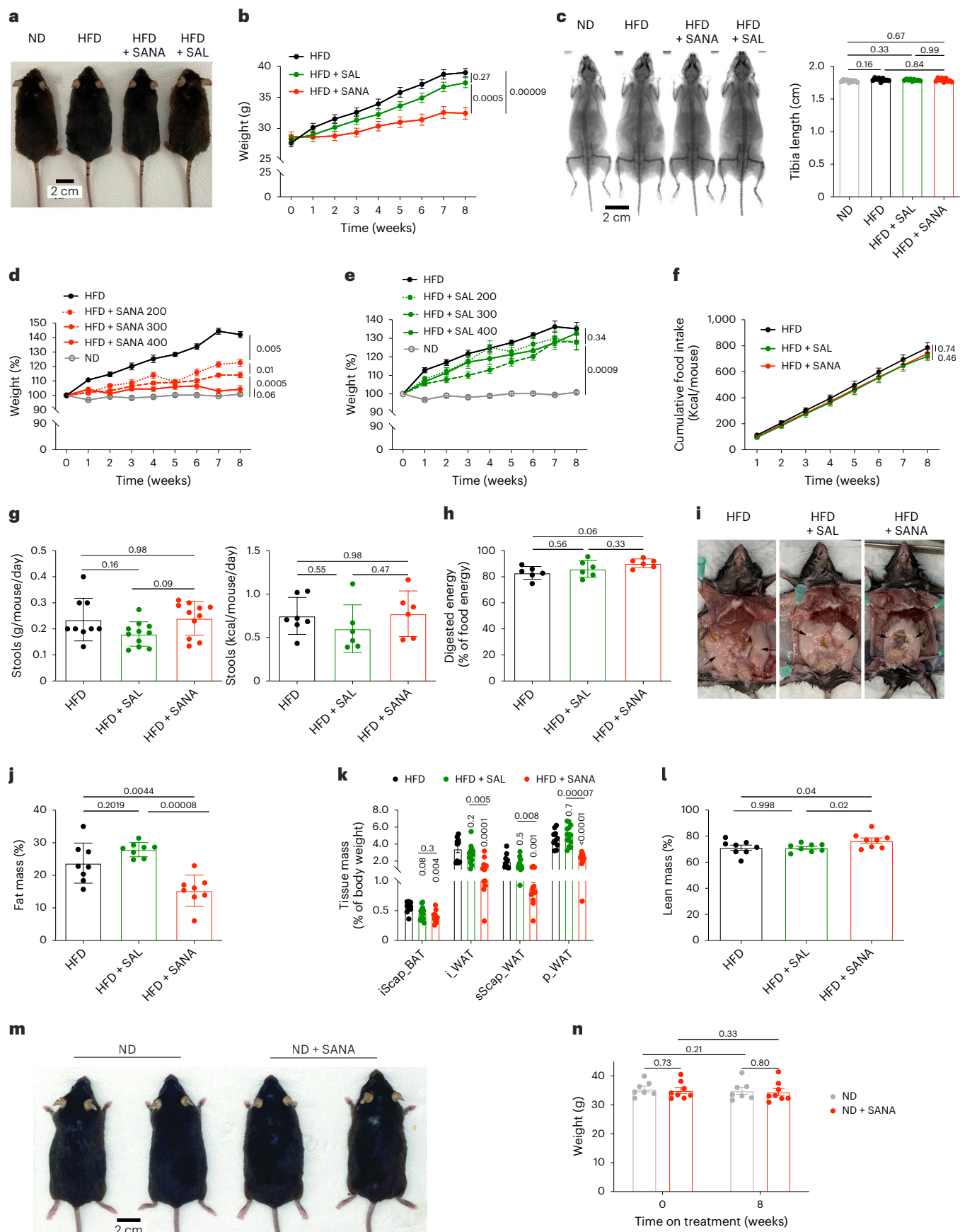
When tested in DIO models, SANA showed unexpected properties for a nitroalkene-based small molecule. Indeed, SANA dramatically protected mice from DIO (Fig. 1a–f), despite not affecting normal growth (Fig. 1c), total food consumption (Fig. 1f), stool mass and calories (Fig. 1g) and digested energy (Fig. 1h) and activity (Extended Data Fig. 2k). Importantly, SANA showed a maximum effect on obesity at doses where the scaffold salicylate was completely ineffective (Fig. 1d,e). Protection against DIO by SANA was due to decreased fat accumulation in all adipose depots analysed (Fig. 1i–k), paralleled by an increase in the percentage of lean mass in the SANA-treated mice (Fig. 1l). SANA showed no effect on body weight on mice fed with normal chow (Fig. 1m,n).

SANA protects mice from DIO-associated metabolic damage

While assessing the metabolic consequences of DIO, we found that the livers of mice fed a high-fat diet (HFD) and treated with SANA had normal macroscopic appearance, indistinguishable from the livers of lean, age-matched control mice (Fig. 2a). Histological analysis of livers confirmed these findings, revealing that mice treated with SANA showed no signs of liver steatosis (Fig. 2b). Examination of livers revealed SANA treatment abrogated DIO-mediated elevation in total liver weight induced by a HFD (Fig. 2c). Analysis of liver transaminases in plasma showed complete protection from obesity-related liver damage (Fig. 2d). Assessment of glucose management after DIO revealed that SANA protected mice from elevated blood glucose levels (Fig. 2e). Furthermore, SANA improved impaired glucose tolerance

Fig. 1 | SANA protects against DIO. **a**, Mice fed HFD, HFD + salicylate (SAL) or HFD + SANA (400 mg per kg per day, mixed in HFD, p.o.) for 8 weeks. **b**, Weight gain. *n*: HFD = 30; HFD + SAL = 29; HFD + SANA = 30; pooled from three experiments. **c**, X-ray image (left) and tibia length (right). *n* = 9 per group. **d, e**, Weight gain under normal diet (ND), HFD or HFD + SANA (**d**) or HFD + SAL (**e**) at different doses administered p.o. *n*: HFD = 8; HFD + SANA 200 mg per kg per day = 6; HFD + SANA 300 mg per kg per day = 8; HFD + SANA 400 mg per kg per day = 10; ND = 8 in **d**, and HFD = 11; HFD + SAL 200 mg per kg per day = 5; HFD + SAL 300 mg per kg per day = 9; HFD + SAL 400 mg per kg per day = 10; ND = 8 in **e**. **f**, Cumulative food intake. *n* = 4 per group. **g**, Stool production (left) and caloric content (right) at week 8. *n*: HFD = 9; HFD + SAL = 11; HFD + SANA = 11 and HFD = 7; HFD + SAL = 6; HFD + SANA = 6, respectively. **h**, Digested energy calculated as the percentage of gross energy intake at week

8. *n* = 6 per group. **i**, Representative images; arrows indicate perigonadal fat. **j**, Total fat mass by EchoMRI. *n* = 8 per group. **k**, Fat depot quantification: interscapular brown (iScap_BAT), inguinal (i_WAT), subscapular (sScap_WAT) and perigonadal (p_WAT) adipose tissue. *n*: iScap_BAT: HFD = 10; HFD + SAL = 14; HFD + SANA = 11; i_WAT: HFD = 10; HFD + SAL = 14; HFD + SANA = 12; sScap_WAT: HFD = 10; HFD + SAL = 14; HFD + SANA = 12 and p_WAT: HFD = 10; HFD + SAL = 13; HFD + SANA = 10. **l**, Total lean mass by EchoMRI. *n* = 8 per group. **m**, Mice fed ND or ND + SANA (400 mg per kg per day, p.o.) for 8 weeks. **n**, Weight at start and end of treatment. *n*: ND = 7; ND + SANA = 8. Data are the mean \pm s.e.m. Statistical tests used were two-way analysis of variance (ANOVA) followed by Tukey's multiple-comparisons test (**b**, **d**, **e**, **f** and **n**), repeated-measures one-way ANOVA (**c**) and one-way ANOVA (**g**, **h**, **j**, **k** and **l**). One-way ANOVA was followed by Bonferroni post hoc for multiple comparisons.



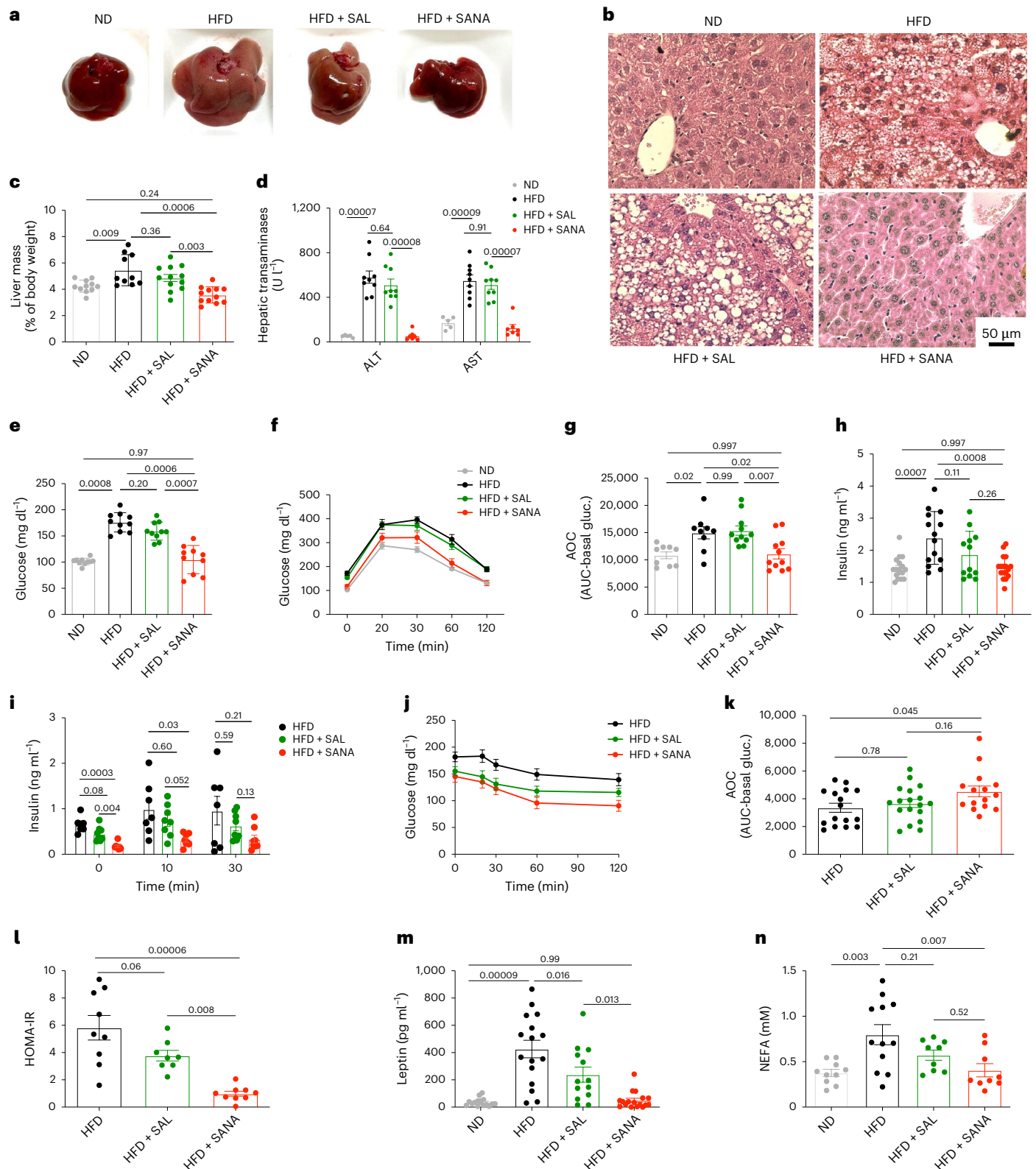


Fig. 2 | SANA protects against glucose intolerance and liver steatosis in response to DIO. a–d, Liver's macroscopic appearance (**a**); H&E staining (**b**); liver weight, *n*: ND = 11; HFD = 10; HFD + SAL = 12; HFD + SANA = 12 (**c**); and liver alanine transaminases (ALT) and aspartate aminotransferase (AST) in plasma/serum, *n*: ND = 5; HFD = 9; HFD + SAL = 9; HFD + SANA = 7 (**d**) in mice fed with ND, HFD, HFD + SAL or HFD + SANA (400 mg per kg per day, p.o.) for 8 weeks. **e–g,** Fasting glucose (**e**) *n* = 10 per group; glucose tolerance test (GTT) (**f**), *n*: ND = 9; HFD = 10; HFD + SAL = 12; HFD + SANA = 11; and GTT area of the curve (AOC) (**g**), *n*: ND = 9; HFD = 9; HFD + SAL = 11; HFD + SANA = 11 at week 8. **h,** Fasting insulin. *n*: ND = 17; HFD = 14; HFD + SAL = 12; HFD + SANA = 17. **i,** Glucose-stimulated insulin secretion

(GSIS) at week 8. *n*: HFD = 7; SAL = 8; SANA = 8. **j,k,** Insulin tolerance test (ITT) (**j**) and ITT AOC (**k**) at week 8. *n*: HFD = 16; HFD + SAL = 18; HFD + SANA = 15 (**l**). Insulin resistance calculated by HOMA-IR. *n*: HFD = 9; HFD + SAL = 8; HFD + SANA = 9. **m,** Plasma leptin levels at week 8. *n*: ND = 16; HFD = 16; HFD + SAL = 13; HFD + SANA = 17. **n,** Plasma non-esterified fatty acid (NEFA) levels at week 8. *n*: ND = 10; HFD = 12; HFD + SAL = 9; HFD + SANA = 9. Data are the mean ± s.e.m. Statistical analyses used were one-way ANOVA followed by Bonferroni post hoc for multiple comparisons (**c–e, g, h, j and l–n**) and two-way ANOVA followed by Tukey's multiple-comparisons test (**k**).

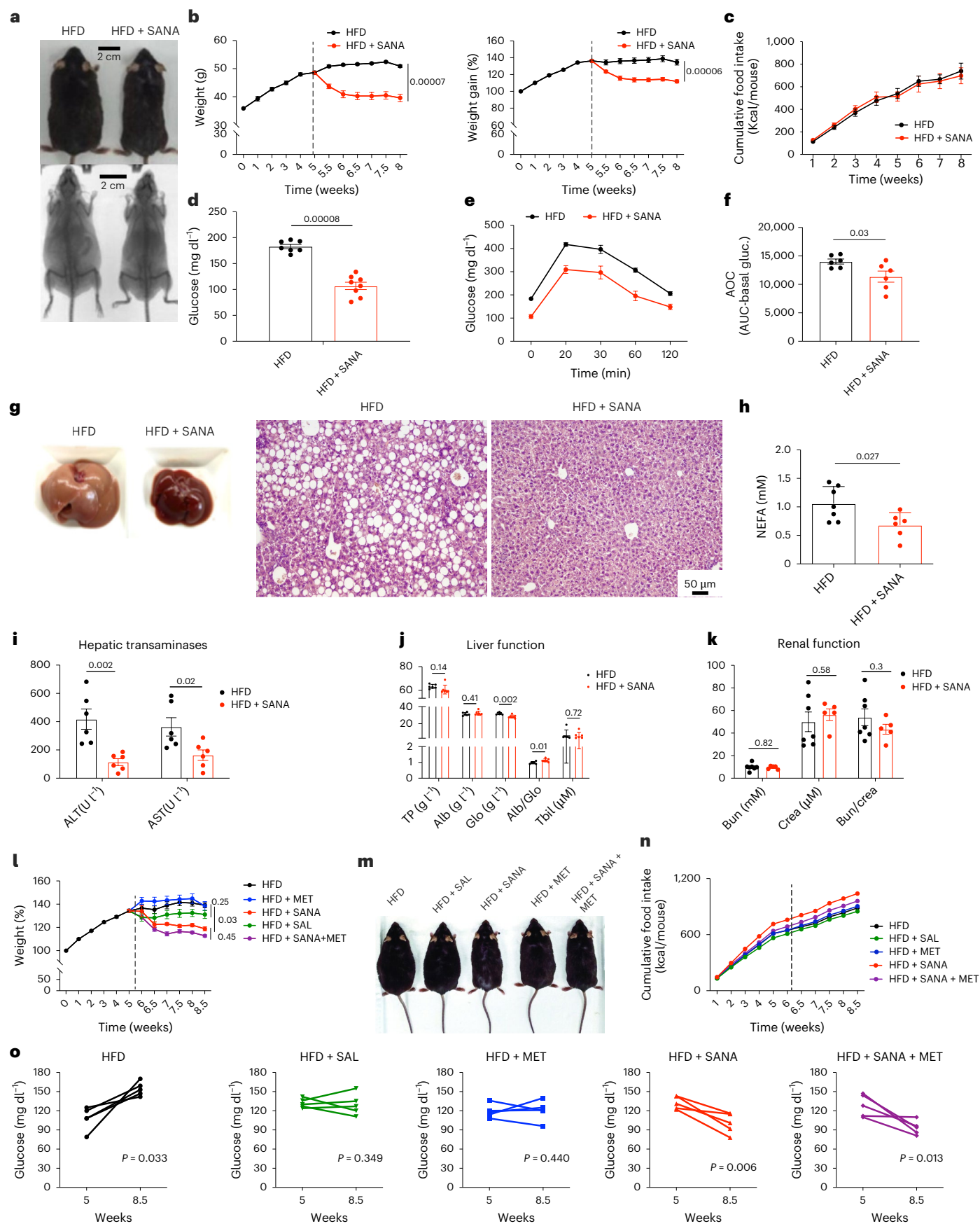


Fig. 3 | Treatment of obese mice with SANA promotes weight loss and

amelioration of glucose intolerance and liver damage. Adult (6-month-old) mice treated with SANA (200 mg per kg per day, p.o.) after 5 weeks of a HFD. **a**, Representative photograph and X-ray image at treatment end. **b**, Weight gain and percentage of initial weight. *n*: HFD = 7; HFD + SANA = 8. **c**, Cumulative food intake during treatment. *n* = 2 per group. **d**, Fasting glucose at week 8. *n*: HFD = 7; HFD + SANA = 8. **e**, **f**, GTT at week 8. *n*: HFD = 6; HFD + SANA = 7 (**e**) and GTT AOC *n* = 6 per group (**f**). **g**, Liver macroscopic appearance and H&E staining. **h**, Plasma free fatty acid levels at week 8. *n*: HFD = 7; HFD + SANA = 6. **i**–**k**, Liver ALT and AST plus liver and renal function markers (TP, total protein; ALB, albumin; GLO, total globulins; TBIL, total bilirubin; BUN, blood urea nitrogen) in plasma/serum

at week 8. Hepatic transaminases: *n* = 6 per group; liver function: *n*: HFD = 6; HFD + SANA = 7; renal function: *n*: HFD = 7; HFD + SANA = 5. **l**, **m**, Percentage of initial weight and representative image of HFD-fed mice treated with SANA or SAL (200 mg per kg per day, p.o.) alone or combined with metformin (MET, 300 mg per kg per day, gavage). *n*: HFD = 5; HFD + MET = 5; HFD + SANA = 5; HFD + SAL = 4; HFD + SANA + MET = 5. **n**, Cumulative food intake. *n* = 2 per group. **o**, Evolution of fasting glucose. *n* = 5 per group. Data are the mean \pm s.e.m. Statistical analyses used were two-way ANOVA followed by Tukey's multiple-comparisons test (**b**, **c** and **l**), unpaired two-sided Student's *t*-test (**d**, **f** and **h**–**k**) and paired two-sided Student's *t*-test (**o**).

and made it indistinguishable from lean age-matched controls and significantly better than obese mice treated with salicylate (HFD + SAL; Fig. 2f,g). Obese mice treated with SANA showed lower insulin levels (Fig. 2h) and a decrease in glucose-induced insulin secretion (Fig. 2i). This was reflected in increased insulin sensitivity as further confirmed (Fig. 2j,k) by HOMA-IR test (Fig. 2l). Leptin and free fatty acid levels were also improved in SANA-treated mice (Fig. 2m,n). Importantly, complete solubilization and pH-dependent stabilization of SANA, followed by once-a-day subcutaneous (s.c.) injection (20 mg per kg per day) provided similar protective effects on weight gain, fasting blood glucose levels and glucose tolerance, with a similar pharmacokinetics profile to oral administration (200 mg per kg per day; Extended Data Fig. 3a–f) and similar levels of SANA in adipose tissue at steady state (Extended Data Fig. 3g). High-performance liquid chromatography (HPLC) and mass spectrometry analysis from plasma showed that metabolism of SANA in vivo led to formation of a saturated form of the molecule 5-(2-nitroethyl)salicylic acid (named metabolite 1, M1; Extended Data Fig. 3h,i). Treatment of mice with M1 had no effect on DIO and glucose management, confirming the need of the reactive nitroalkene group for the metabolic effect of SANA (Extended Data Fig. 3j,k). AMPK activation by salicylate and SANA occurred at similar doses both in vivo and in vitro (Extended Data Fig. 3l,m), and SANA protected against DIO and glucose intolerance in AMPK ($\alpha 1$)-KO mice (Extended Data Fig. 3n,o) indicating that the metabolic effects of SANA are AMPK independent.

SANA is effective in treating obesity and metabolic damage

Addressing DIO and metabolic complications once they are established may be more representative of the clinical need in humans. As such, SANA was administered to adult mice after obesity was established (5 weeks of HFD). SANA-treated mice lost weight (Fig. 3a,b) while cumulative food intake was not affected (Fig. 3c), demonstrated diminished basal glycaemia (Fig. 3d), showed amelioration of glucose intolerance (Fig. 3e,f) and showed no signs of hepatic steatosis (Fig. 3g), decreased free fatty acids in plasma (Fig. 3h) and protection against increased liver enzymes, while no changes in other liver or kidney functional parameters were observed in both groups (Fig. 3i–k). Importantly, SANA (200 mg per kg per day) not only promoted weight loss, but also showed increased effectiveness compared to salicylate (200 mg per kg per day) and metformin (300 mg per kg per day) in glycaemic control during the 3-week period studied (Fig. 3l–o).

Fig. 4 | Proteomic analysis of whole tissue and isolated mitochondria from iWAT to SANA. **a**–**d**, Whole iWAT proteomics performed in mice fed with HFD or HFD + SANA (400 mg per kg per day, p.o.) for 8 weeks. *n* = 3 per group. **a**, Heat map displaying unique proteins per row (labels shown every third protein) across biological replicates. **b**, Venn diagram of proteins exclusively detected in each condition ($P < 0.05$), including CKM. **c**, Volcano plot of common proteins with differential abundance (Benjamini–Hochberg $q < 0.05$); each dot represents a protein detected in at least four of six replicates; darker dots are statistically differential, and red dots are mapped to the enriched biological processes in **d**.

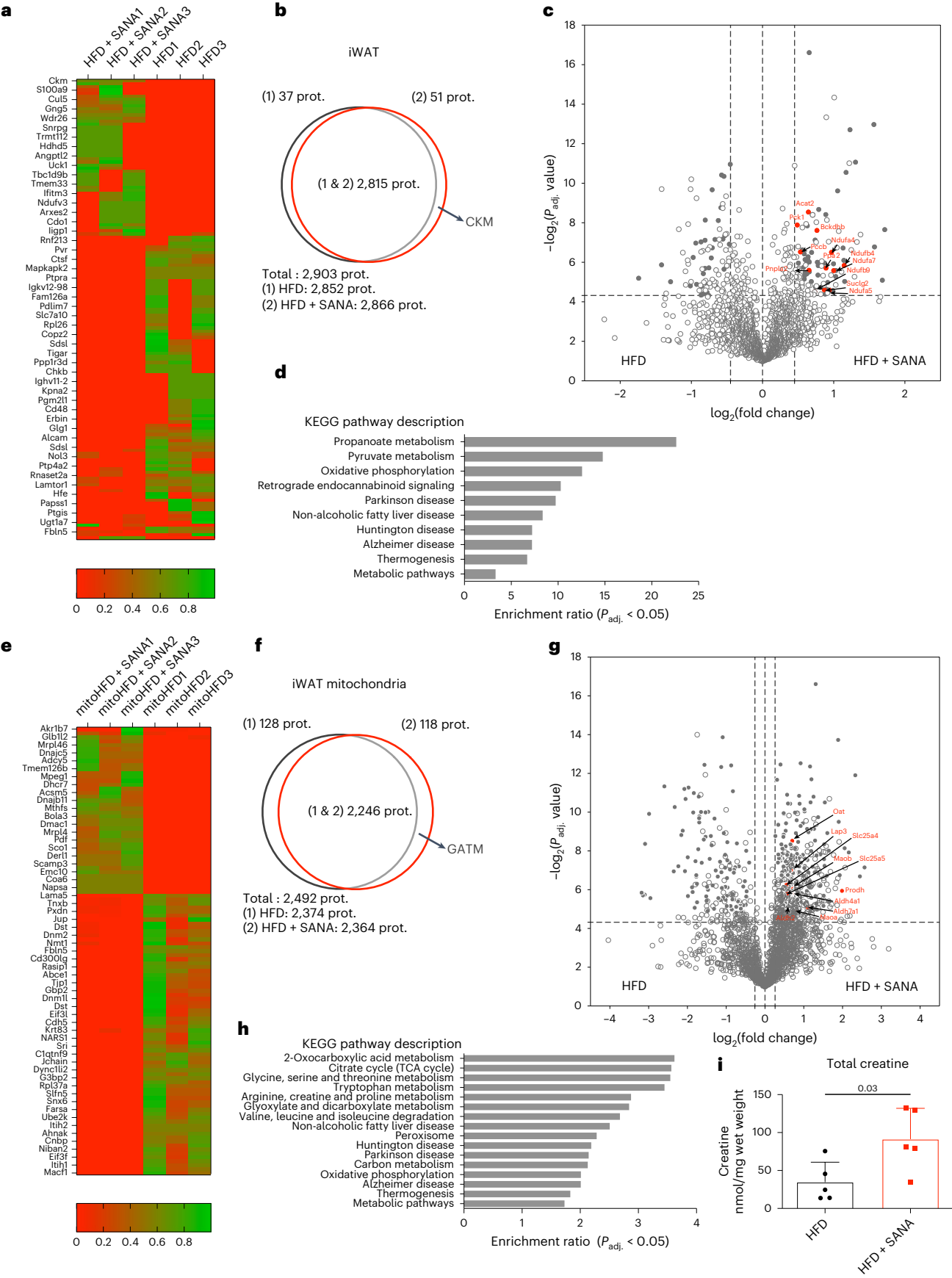
Proteomic analysis in iWAT shows that SANA induces thermogenesis

The phenotype triggered by SANA pointed to increased energy expenditure in adipose tissue as a putative mechanism of action. Based on the recent emergence of alternative thermogenic pathways, we used unbiased proteomic analysis in iWAT as a discovery approach. Label-free quantitative proteomic analysis in iWAT of mice revealed a consistent shift in the pattern of protein expression between obese mice and obese mice treated with SANA (Fig. 4a). Proteins uniquely detected in HFD or HFD + SANA, as well as those differentially abundant between conditions were pinpointed (Fig. 4b,c and Supplementary Table 1). Combined, 109 proteins were increased in HFD + SANA iWAT tissue. Kyoto Encyclopedia of Genes and Genomes pathway enrichment analysis showed that SANA stimulated catabolism, oxidative phosphorylation and thermogenesis (Fig. 4d and Supplementary Table 1). Next, we extended the proteomic analysis to isolated mitochondria from iWAT. Heat map and differential analyses from mitochondrial proteomes showed a dramatic change in the protein expression profile in SANA-treated compared to placebo-treated animals (Fig. 4e–g and Supplementary Table 1). In this case, 380 proteins were identified as statistically overrepresented in HFD + SANA (Fig. 4f,g). Pathway enrichment analysis showed that thermogenic, metabolic and tricarboxylic acid cycle, arginine-related, glycine-related and proline-related metabolic pathways were upregulated by SANA (Fig. 4h and Supplementary Table 1). These results resembled those previously described¹⁹ after cold-induced thermogenesis in mice and pointed to an increased activity of the creatine-dependent thermogenesis. Interestingly, among the proteins detected only after SANA treatment, glycine amidinotransferase (GATM), the rate-limiting step in creatine synthesis (Fig. 4f), and creatine kinase M-type (CKM) were present (Fig. 4b). Consistent with the metabolic signature of creatine-dependent thermogenesis described previously¹⁹ and the upregulation of GATM (Fig. 4f), we found a significant increase in creatine levels in iWAT from SANA-treated mice (Fig. 4i).

SANA stimulates creatine-dependent thermogenesis

In line with the proteomic signature, thermal images showed that SANA-treated mice had increased surface temperature (Fig. 5a). Tissue microscopic analysis in iWAT showed an appearance of interspaced adipocytes with decreased lipid droplet size, consistent with a beige phenotype (Fig. 5b). Indeed, SANA stimulated

d, WebGestalt pathway over-representation analysis for proteins overexpressed in HFD + SANA versus HFD. **e**–**h**, Same proteomic analysis conducted on isolated mitochondria from iWAT, highlighting mitochondrial GATM. *n* = 3 per group; each sample is pooled from 2–3 mice. **i**, Total creatine levels in iWAT were measured by mass spectrometry. *n* = 5 per group. Data are the mean \pm s.e.m. Statistical analyses used were Bayesian framework with a Poisson distribution to identify exclusively detected proteins (**b** and **f**), multiple unpaired two-sided Student's *t*-tests (one per protein) for volcano plots (**c** and **g**) and an unpaired two-sided Student's *t*-test (**i**).



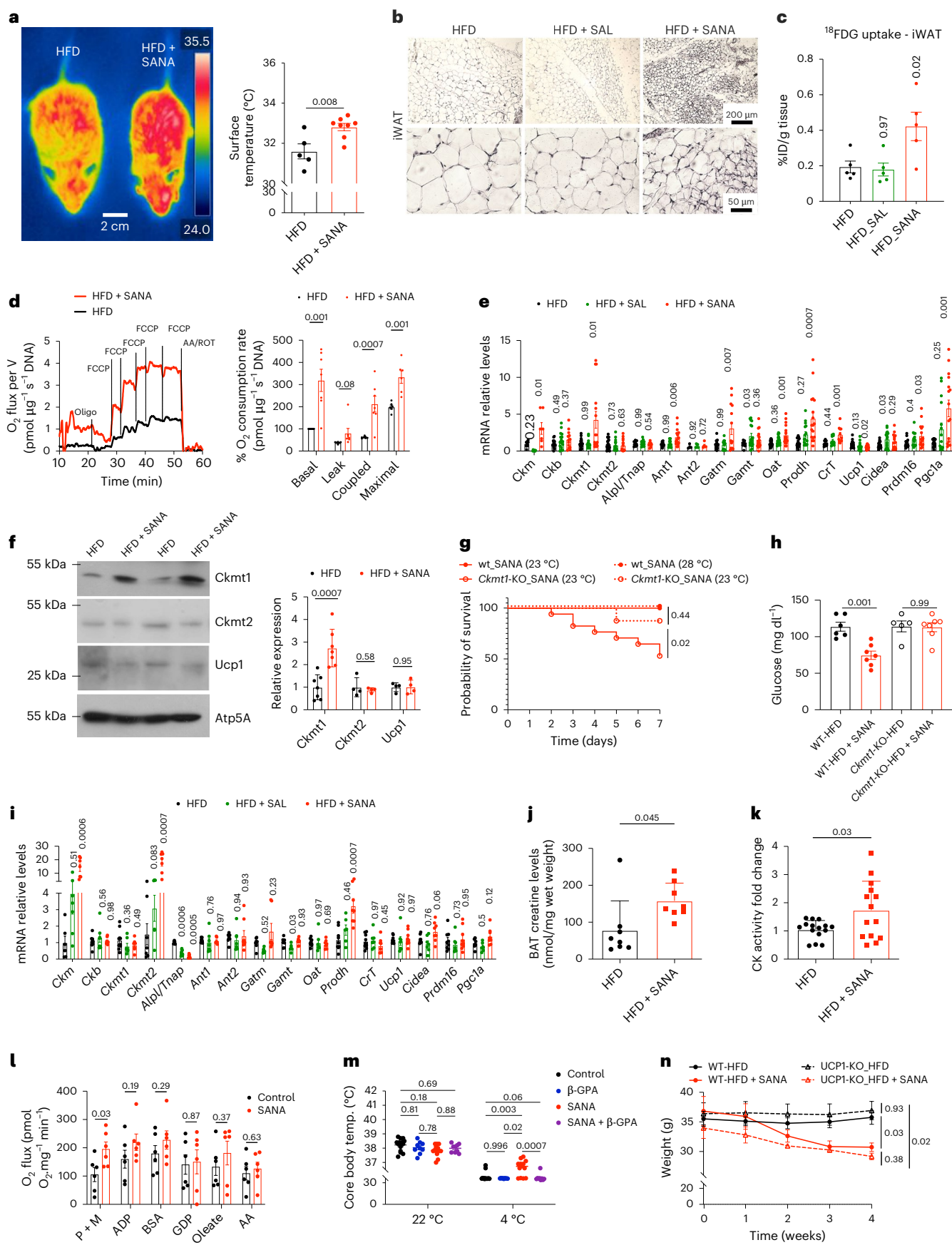


Fig. 5 | SANA stimulates mitochondrial respiration, a gene expression signature of creatine-dependent thermogenesis and a UCPI-independent loss of weight. **a–f, i–k**, Measurements at 8 weeks of treatment in mice fed with HFD, HFD + SANA or HFD + SAL at 400 mg per kg per day, p.o. **a**, Thermal images (left), with inguinal surface temperatures quantification (right). *n*: HFD = 5; HFD + SANA = 8. **b**, Representative H&E staining of iWAT. **c**, In vivo ^{18}F FDG uptake in iWAT. *n* = 5 per group. **d**, Oxygen consumption of adipocytes isolated from iWAT. *n* = 7 per group. **e**, Quantitative PCR with reverse transcription (RT–qPCR) analysis of thermogenic markers in iWAT. *n*: Supplementary Table 1. **f**, Western blot of iWAT-isolated mitochondria, *n* = 7 for CKMT1; *n* = 4 for CKMT2 and UCPI. **g**, Survival curves for WT and *Ckmt1*-KO mice treated with HFD + SANA (20 mg per kg per day, s.c.) at 23 °C or 28 °C. *n*: wt_SANA_23 °C = 6; *Ckmt1*-KO_SANA_23 °C = 17; wt_SANA_28 °C = 7; *Ckmt1*-KO_SANA_28 °C = 8. **h**, Fasting glucose in WT and *Ckmt1*-KO mice at 28 °C after HFD and SANA or vehicle treatment. *n*: WT-HFD = 6; WT-HFD + SANA = 7; *Ckmt1*-KO-HFD = 5; *Ckmt1*-KO-HFD + SANA = 7. **i**, RT–qPCR analysis of thermogenic markers in BAT, *n*: Supplementary Table 1. **j**, Total creatine levels in BAT measured by

mass spectrometry. *n* = 8 per group. **k**, Creatine kinase activity in BAT-isolated mitochondria, *n*: HFD = 15; HFD + SANA = 14. **l**, Respiration analysis in BAT-isolated mitochondria. *n* = 6 per group. **m**, β -GPA treatment (0.4 mg per kg per day, i.p.) in SANA-treated mice for 5 days (20 mg per kg per day, s.c.) before a 3-h cold exposure. *n*: Control = 14; β -GPA = 9; SANA = 13; SANA + β -GPA = 9. **n**, Weight gain of UCPI-KO mice treated with SANA (20 mg per kg per day, s.c.) or vehicle daily for 4 weeks. Mice were maintained at thermoneutrality and fed with a HFD 15 weeks before treatment. *n* = 5 per group. Mitochondrial assays utilized oligomycin (oligo), FCCP (carbonyl cyanide *p*-trifluoromethoxyphenylhydrazone), antimycin A (AA), rotenone (ROT), pyruvate (P), malate (M) and fatty acid-free BSA. Data are the mean \pm s.e.m. Statistical analyses used were paired two-sided Student's *t*-test (**a**), unpaired two-sided Student's *t*-tests (**d**, **f** and **j–l**), one-way ANOVA followed by Bonferroni post hoc for multiple comparisons (**c**, **e** and **l**), two-way ANOVA followed by Tukey's multiple-comparisons test (**h**, **m** and **n**) and log-rank (Mantel–Cox) test (**g**). Vertical *P* values indicate multiple comparisons of each experimental condition versus the control condition (HFD in **c**, **e** and **l**).

^{18}F -fluoro-2-deoxyglucose (^{18}F FDG) uptake in vivo in iWAT (Fig. 5c). However, with the exception of the brain, glucose uptake in other tissues was not affected by SANA treatment (Extended Data Fig. 4a). Isolated inguinal white adipocytes from mice treated with SANA for 8 weeks demonstrated increased mitochondrial respiration (Fig. 5d), consistent with the signature from tissue proteomic data. SANA also induced increased respiration when human intact differentiated adipocytes were treated for 24 h (Extended Data Fig. 4b). However, direct treatment of adipocytes, isolated mitochondria from iWAT or brain with SANA had no direct effect on mitochondrial respiration (Extended Data Fig. 4c–e), demonstrating the effect of SANA on adipocyte respiration is delayed and potentially mediated by a genomic mechanism rather than acute regulation of mitochondrial respiration. Therefore, next we explored the possibility that SANA could induce changes in gene expression profiles in mouse iWAT. In fact, we observed that SANA stimulated the expression of *Ckmt1* and *Ckm* (Fig. 5e). Importantly, the increase in mRNA for *Ckmt1* was also reflected on increased CKMT1 protein levels (Fig. 5f). Other genes involved in creatine metabolism, transport and synthesis including *Slc25a4* (*Ant1*), *Gatm*, *Oat*, *Prodh* and *Slc6a8* (*CrT*) were also upregulated by SANA (Fig. 5e). In contrast, *Ucp1* was downregulated in mice treated with SANA when measured by mRNA (Fig. 5e), but no significant changes were observed in UCPI protein levels by western blot (Fig. 5f). The thermogenesis-related genes *Cidea*, *Prdm16* and *Ppargc1a* (*Pgc1a*) were also upregulated by SANA (Fig. 5e). Importantly, treatment of differentiated human white adipocytes with SANA stimulated the expression of regulators of creatine metabolism, including CKMT1 and CKMT2 (sarcomeric mitochondrial CK; Extended Data Fig. 4b). Surprisingly, we found that *Ckmt1*-KO mice treated with SANA showed a ~50% increase in mortality rate after 1 week of treatment (no mortality occurred in wild-type (WT) mice), an effect that was rescued when *Ckmt1*-KO mice were acclimatized at thermoneutrality during the treatment with SANA (Fig. 5g). Under thermoneutral conditions, the glucose-lowering effect of SANA was lost in *Ckmt1*-KO mice (Fig. 5h), showing that SANA may require CKMT1 for its effects on

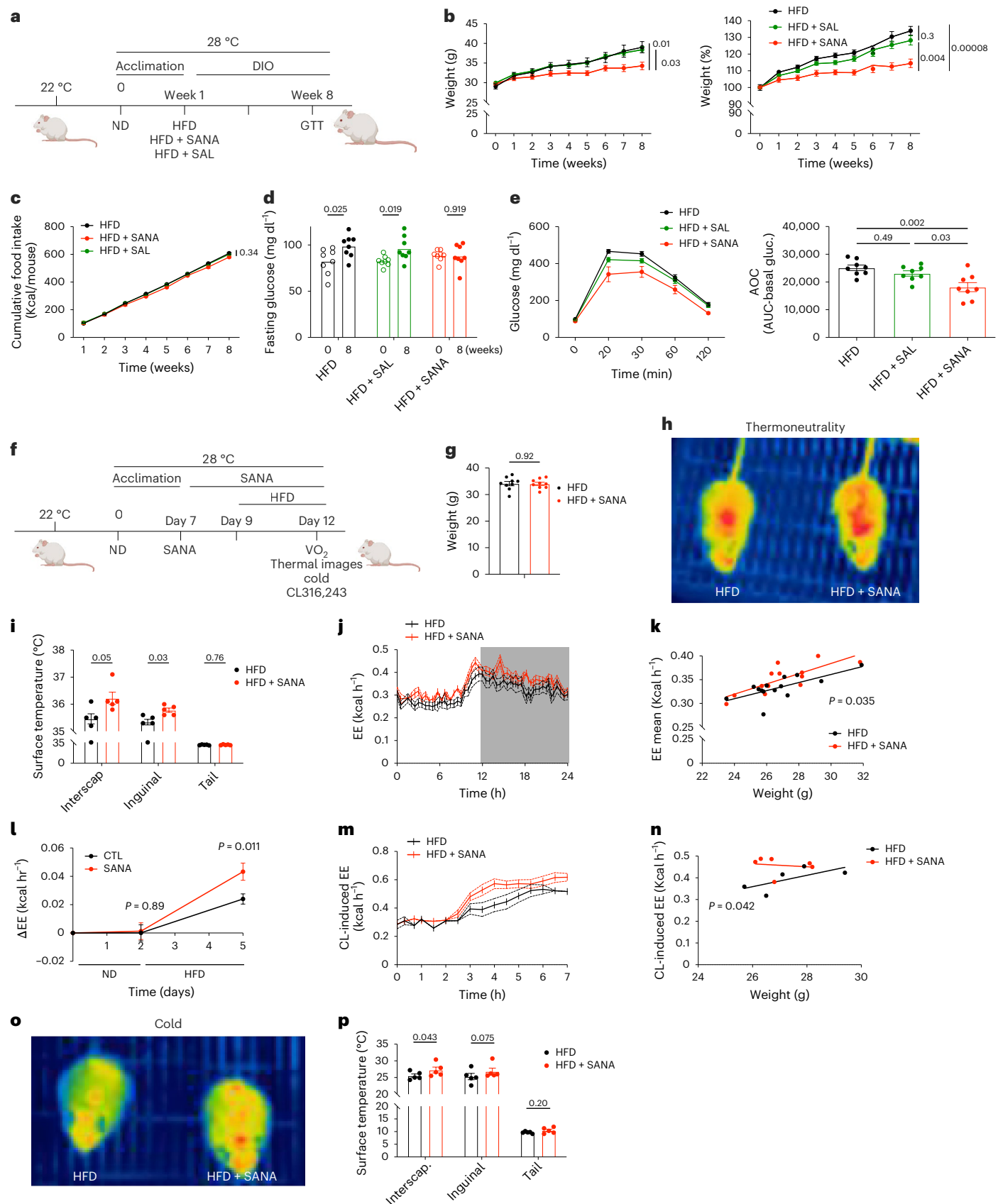
glucose homeostasis and thermoregulation in vivo. SANA also stimulated the expression of genes involved in creatine metabolism and thermogenesis in brown adipose tissue (BAT). Unlike in iWAT, where *Ckm* and *Ckmt1* expression is upregulated by SANA, in BAT *Ckm* and *Ckmt2* increased in expression (Fig. 5e, i). Other thermogenesis-related genes such as *Cidea*, *Pgc1a*, *Gatm* and *Prodh* were upregulated in BAT, whereas *Ucp1* was not altered (Fig. 5i). These changes in gene expression profile in BAT were reflected by increased creatine (Fig. 5j) and creatine kinase activity in isolated mitochondria (Fig. 5k). Measurements of respiration in isolated mitochondria of animals treated with SANA showed increased state II respiration (Fig. 5l). However, BAT mitochondrial respiration inhibited by GDP (Fig. 5l and Extended Data Fig. 4f) and stimulated after titration with oleate (Fig. 5l), attributable to UCPI activity²⁰, was not altered by SANA. Although not quantitative, these effects support the notion that increased state II respiration was not dependent on UCPI regulation. Direct addition of SANA to BAT-isolated mitochondria also had no effect on GDP-inhibited respiration (Extended Data Fig. 4g). We further confirmed these findings by treating obese UCPI-KO mice with SANA and found that the compound promoted weight and fat mass loss (Fig. 5n and Extended Data Fig. 4h–j) without affecting food consumption (Extended Data Fig. 4h). To further support the thermogenic potential of SANA, we performed cold challenge experiments. Mice treated with SANA (20 mg per kg body weight, s.c., for 5 days) exposed to cold showed improved thermogenic response compared to controls (Extended Data Fig. 4k), which was reflected in upregulation of creatine kinases and thermogenic markers (Extended Data Fig. 4l) and increased creatine levels in iWAT (Extended Data Fig. 4m). To confirm that the improved response to cold was dependent on creatine, mice were treated with the creatine-depleting drug β -guanidinopropionic acid (β -GPA)²¹, which can only be used acutely as chronic exposure can induce weight loss^{19,21}. Mice were treated with SANA (20 mg per kg per day, s.c.) or SANA + β -GPA daily (0.4 mg per kg per day, intraperitoneally) for 5 days. Treatment with β -GPA abolished the effect of SANA on thermogenic response

Fig. 6 | SANA stimulates energy expenditure and protects against obesity under thermoneutral conditions. **a**, Diagram of long-term treatment: Mice were fed HFD, HFD + SAL or HFD + SANA (20 mg per kg per day, s.c.) for 8 weeks. Created with BioRender.com. **b**, Weight gain and percentage of initial weight. *n*: HFD = 13; HFD + SAL = 10; HFD + SANA = 11. **c**, Cumulative food intake. *n* = 2 per group. **d**, Fasting glycaemia at weeks 0 and 8. *n* = 8 per group. **e**, GTT (left) and GTT AOC (right) at week 8. *n* = 8 per group. **f**, Diagram of acute treatment. Mice were given a HFD with or without SANA (20 mg per kg per day, s.c.) at 28 °C. Created with BioRender.com. **g**, Body weight. *n* = 9 per group. **h**, Representative thermal image of HFD and HFD + SANA mice at the end of the acute treatment. **i**, Quantification of surface temperature from thermal images. *n* = 5 per group. **j–l**, Energy expenditure (EE) evaluations from the acute treatment. *n*: HFD = 14;

HFD + SANA = 13; data were pooled from two independent experiments. **j**, EE measured over a 24-h period. **k**, Regression analysis of EE data from **j**. **l**, Individual changes in EE during the acute treatment. **m, n**, EE evaluations of CL316,243-treated mice at the end of the acute treatment. *n*: HFD = 5; HFD + SANA = 6 (**m**) EE measurement. **n**, Regression analysis of EE from **m**. **o, p**, Thermoneutral-to-cold (4 °C) challenge. Representative thermal image after 1 h at 4 °C (**o**). Surface temperature quantification from images (**p**). *n* = 5 per group. Data are the mean \pm s.e.m. Statistical analyses used were one-way ANOVA followed by Bonferroni post hoc for multiple comparisons (**e**), two-way ANOVA followed by Tukey's multiple-comparisons test (**b** and **c**), paired two-sided Student's *t*-test (**d**, **i** and **p**), unpaired two-sided Student's *t*-test (**g** and **l**) and ordinary least squares and ANCOVA for regression analyses (**k** and **n**).

(Fig. 5m), confirming that creatine is necessary for the effect of SANA on thermogenesis. No changes in body weight or food consumption were detected among treatments (Extended Data Fig. 4n,o). Muscle activity was also assessed during cold exposure. As creatine is a major muscle

metabolite, we tested the potential for SANA to affect muscle function. Electromyographic analysis showed that shivering thermogenesis was not affected by SANA (Extended Data Fig. 5a). Creatine kinase expression and mitochondrial function in skeletal muscle and cells



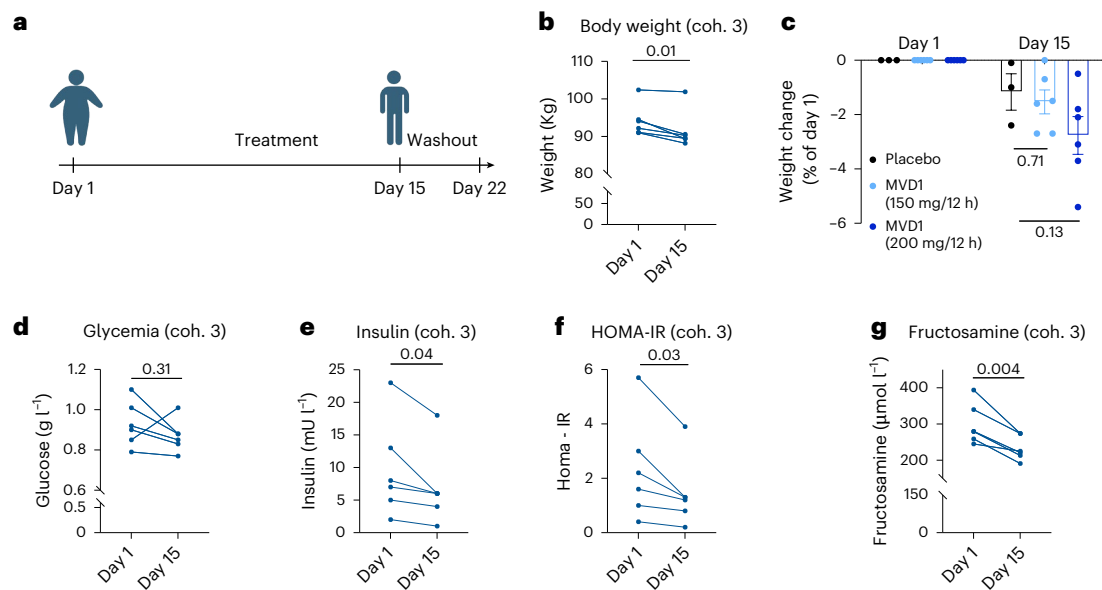


Fig. 7 | Study design and main metabolic parameters induced by SANA (under the name of MVD1 during clinical studies) in a randomized, double-blind, placebo-controlled study phase 1A/B, first-in-human clinical trial in healthy volunteers with overweight or obesity. **a**, Clinical scheme of trial design for MAD. The complete design for SAD and MAD is described in Extended Data Fig. 8. Created with BioRender.com. **b**, Analysis of weight evolution in the MAD cohort 3 between day 1 and day 15. $n = 6$ per group. All remaining data for all cohorts can be found in Extended Data Table 1. **c**, Analysis of percentage of body weight loss

between day 1 and day 15 in placebos and treated volunteers in MAD (cohort 2 and cohort 3). n : Placebo = 3; MVD1 150 mg/12 h = 6; MVD1 200 mg/12 h = 6. Data are presented as the mean \pm s.e.m. **d–g**, Analysis of plasma glucose (**d**), insulin levels (**e**), HOMA-IR test (**f**) and fructosamine levels (**g**), comparing day 1 and day 15 of MAD cohort 3 volunteers treated with MVD1 200 mg/12 h. $n = 6$. All remaining data for all cohorts can be found in Extended Data Table 1. Statistical analyses used were paired two-sided Student's t -test (**b** and **d–g**) and one-way ANOVA followed by Bonferroni post hoc for multiple comparisons (**c**).

were not affected by SANA (Extended Data Fig. 5b–d), although there was a significant increase in muscle creatine levels in vivo (Extended Data Fig. 5e). Aerobic exercise capacity was performed and revealed that SANA did not impact muscle physiology (Extended Data Fig. 5f). Furthermore, treatment with SANA did not generate any observable deleterious effects on cardiac mitochondrial respiration (Extended Data Fig. 5g) or function (Extended Data Fig. 5h).

SANA stimulates energy expenditure during thermoneutrality

One caveat of envisioning thermogenesis as a suitable approach to treat obesity in humans is that they spend most of their time under thermoneutral conditions. Interestingly, disruption of creatine metabolism in adipose tissue decreases energy expenditure and promotes obesity in thermoneutrality^{22,23}. Administration of SANA under thermoneutral conditions (Fig. 6a) also protected against DIO (Fig. 6b), with no effect on accumulated food intake (Fig. 6c). SANA was also effective in preventing diet-induced hyperglycaemia (Fig. 6d) and glucose intolerance (Fig. 6e), further supporting that SANA may be a suitable treatment for obesity under thermoneutral conditions. To clearly determine that increased energy expenditure due to thermogenesis is a driving force for the protection against obesity but not a side effect of differences in body weight, we followed a protocol of acute HFD feeding (Fig. 6f) as previously described²³. During this short treatment there was no difference in weight gain among groups (Fig. 6g). However, thermal imaging showed that SANA promoted an increase in body heat dissipation (Fig. 6h,i). Consistently, mice treated with SANA during acute HFD feeding showed a significant increase in energy expenditure (Fig. 6j–l). These results are consistent with previous reports showing that a HFD is necessary for activation of creatine metabolism and energy expenditure in adipose tissue²³. Interestingly, treatment of mice with SANA fed with normal chow showed no changes in energy expenditure (Extended Data Fig. 6). To further confirm our results, we administered the β_3 -adrenergic agonist CL316,243 after 3 days of acute HFD feeding.

Single treatment with CL316,243 stimulated a transient increase in energy expenditure, which was significantly increased in SANA-treated mice, irrespective of body weight, as shown by analysis of covariance (ANCOVA) analysis (Fig. 6m,n). Additionally, after acute HFD feeding at 28 °C, the mice were exposed to cold and surface temperature was assessed. Mice treated with SANA showed increased heat dissipation measured by thermal imaging (Fig. 6o,p). Finally, we used the acute HFD model to explore the effect of SANA isomers and analogues on creatine-dependent thermogenesis. We synthesized two different SANA isomers, 3-(2-nitroethenyl)salicylic acid and 4-(2-nitroethenyl)salicylic acid. In these isomers, the nitroalkene group was linked to the carbons 3 and 4 of salicylate, respectively, and 5-(2-nitroallyl)salicylic acid, with an extended carbon chain. We named them 3-SANA, 4-SANA and E-SANA, respectively (Extended Data Fig. 7a). SANA analogues were tested for their capacity to induce thermogenic response under acute HFD treatment (Extended Data Fig. 7a). Of all the compounds tested, only SANA activated thermogenesis, measured by infra-red imaging (Extended Data Fig. 7b,c) or increased the expression of creatine kinases in BAT (Extended Data Fig. 7d), showing that not only is the effect dependent on the presence of nitroalkene, but also the location is crucial for its function.

Analysis of safety and pharmacodynamics of SANA in human volunteers

Based on all the accumulated preclinical evidence supporting that SANA might be a suitable first-in-class drug for treatment of obesity and comorbidities, we performed a randomized, double-blind, placebo-controlled phase 1A/B clinical trial in healthy lean volunteers and in volunteers with obesity. A single ascending dose (SAD; total cohort size of 17 volunteers) and a multiple ascending dose (MAD; total cohort size of 24 volunteers) were evaluated in lean and volunteers with obesity, respectively (Extended Data Figs. 7a and 8a). For clinical development purposes, SANA was referred to as MVD1. The primary endpoint of the study was to determine the safety of MVD1. Secondary

Table 1 | Summary of the AEs reported during SAD and MAD

	Treated participants	Participants with possibly drug-related AEs	Participants with definitively drug-related AEs
SAD cohort (dose)	<i>n</i>	<i>n</i>	<i>n</i>
1 (200 mg)	4	0	0
2 (400 mg)	4	3 ^a	0
3 (800 mg)	3	0	2 ^b
MAD cohort (dose)	<i>n</i>	<i>n</i>	<i>n</i>
1 (200 mg)	6	5 ^c	0
2 (300 mg)	6	4 ^d	0
3 (400 mg)	6	5 ^e	0

^aOne participant with mild, self-resolving diarrhoea, one with headache and one with tiredness. Mild, self-resolved AEs. ^bTwo with renal tubular damage, one of whom also had nausea and mild, self-resolving diarrhoea. Mild, self-resolved AEs. ^cTwo with headache, two with loose stools and one with lightheadedness. Mild, self-resolved AEs. ^dOne with headache, one with mild, self-resolving diarrhoea, one with abdominal pain and one with dysphagia. Mild, self-resolved AEs. ^eOne with constipation, one with soft stools, two with headaches and one with increased thirst. Mild, self-resolved AEs.

endpoints included tolerability and pharmacokinetics. Additionally, exploratory endpoints (that is, body weight, glucose and insulin) were also analysed during the MAD part of the study. The demographic and baseline characteristics of the cohorts are presented in Extended Data Table 1. Regarding the safety of MVD1, only two patients showed adverse events (AEs) that were interpreted to be definitively related to the drug (renal reversible tubular damage, evidenced by proteinuria and glucosuria), which occurred with the highest dose of the SAD. No definitively drug-related AEs were observed during the MAD. One patient that was withdrawn from MAD cohort 1 (Fig. 7a) was later determined to have a pre-existing condition (Methods). A summary of the patients with at least one possible or definitively drug-related AE is presented in Table 1. The most frequent possibly drug-related AEs were headache or soft stools. No severe AEs were observed during the study (both SAD and MAD). Liver function was normal in all patients after 15 days of treatment (Supplementary Table 1). Pharmacokinetics profiles both in SAD and MAD were like the ones determined in mice (Extended Data Fig. 8c,d and Supplementary Table 1). Importantly, a pharmacokinetics profile in day 15 of MAD was comparable to day 1, showing that drug does not accumulate in the body over time (Extended Data Fig. 8d and Supplementary Table 1).

Finally, we analysed the exploratory endpoints of the study during the MAD. The MAD study was carried as an inpatient study, and all meals containing a high-carbohydrate diet (250–300 g per day) were provided ad libitum to the volunteers (see meal plan in the Methods). The body weight and glucose metabolism marker evolution for all cohorts and placebos is presented in Extended Data Table 1. Although the study was designed and powered to determine safety and tolerability, when we analysed volunteers in cohort 3 (200 mg/12 h) we found that volunteers with overweight or obesity showed a significant decrease in body weight in 15 days of treatment (Fig. 7b). Indeed, volunteers showed weight loss of about 3% at maximum dose (Fig. 7c), which is comparable to the weight loss found for semaglutide after the same period of treatment². Furthermore, the volunteers not only lost weight, but also showed improvement in glucose metabolism. Except for one, all volunteers at 200 mg/12 h showed amelioration of plasma glucose (Fig. 7d). Insulin levels (Fig. 7e) and insulin resistance (HOMA-IR) were significantly improved during the treatment with 200 mg/12 h (Fig. 7f). Importantly, fructosamine levels, which is a read-out of average blood glucose levels over the past 2–3 weeks, was significantly improved in all MAD 3 cohort (200 mg/12 h) volunteers during the period of treatment (Fig. 7g). Volunteers treated with placebo did not show any

effect in these parameters (Extended Data Table 1). One volunteer started the study with a body weight of 102.40 kg and ended with 101.90 kg. Interestingly, the initial glucose and insulin were 1.01 g l⁻¹ and 23 mU l⁻¹, ending in 0.88 g l⁻¹ and 18 mU l⁻¹, respectively. In consequence, the HOMA-IR improved from 5.7 to 3.9. Although preliminary, these results suggest that SANA may promote improvement of the glucose–insulin axis independently of body weight. This topic warrants further investigation. Overall, even though the clinical study was designed to determine safety and tolerability, the clinical data show that SANA not only is safe and well tolerated but also appears to have promising salutary clinical results in patients with obesity.

Discussion

Obesity and its metabolic complications are a challenging problem for pharmaceutical interventions. The multifactorial causes of obesity, and the need for long-term interventions with associated side effects highlight the necessity for constant pharmacological innovation. The irruption of the GLP-1 mimetics provides hope for effective and safe treatments for obesity²⁴. However, the massive use of GLP-1 agonists is under pharmacological surveillance, and evidence about long-term safety, efficacy and compliance is still being collected. As an example, gastrointestinal effects, such as gastroparesis, nausea and diarrhoea, are among the side effects of GLP-1 treatment that call for attention²⁵. Also, some concerns about sarcopenia exist, although more definitive data are still missing²⁶. In that sense, developing alternative and even complementary approaches is of need. The use of hybrid drugs based on well-designed modifications of safe and inexpensive compounds may offer a suitable way to provide massive, safe and affordable therapies for this pandemic disease.

The current study addressed the effects of a derivative of the ancient and long-time-used drug salicylate, 5-(2-nitroethenyl) salicylic acid, on the prevention and treatment of DIO and its related metabolic abnormalities. The data demonstrate that: (1) SANA is effective for weight loss and weight gain prevention during DIO, but not under normal diet; (2) the primary metabolic abnormalities associated with obesity are improved by SANA; (3) the beneficial effects of SANA are substantially greater than those obtained with salicylate; (4) the effects of SANA are mediated by stimulation of mitochondrial respiration in intact adipocytes in vivo, but not in isolated mitochondria in vitro; (5) SANA protects against DIO at thermoneutral conditions, a situation closely related to normal human environmental conditions; and (6) SANA is safe and well tolerated in healthy lean volunteers and also in individuals with overweight or obesity, showing promising effects in weight and glucose management in a 15-day-long trial.

Our analysis of adipose tissue indicated that the salutary effects of SANA are associated with stimulation of non-shivering thermogenesis, a homeostatic mechanism present in all mammals, which constitutes an attractive approach for treating obesity²⁷. Several reports show that adipose tissue-dependent thermogenesis is stimulated in humans after cold exposures^{28,29}. Importantly, the effects mediated by SANA occur through an increase in creatine-related energy expenditure, reminiscent of creatine-dependent thermogenesis, or futile creatine cycle^{30,31}, a heat-production pathway that can maintain body temperature in the complete absence of UCP1 expression³². Recent studies have demonstrated that the futile creatine cycle plays a significant role in thermogenesis, functioning alongside UCP1 in both brown and beige adipocytes^{32–35}. SANA stimulates thermogenesis independently of UCP1 expression or activation (Fig. 5) and does not directly uncouple mitochondria. Salicylate, the precursor of SANA, promotes thermogenic activity in murine BAT by UCP1-dependent and UCP1-independent mechanisms^{12–14,36}. The latter involves direct uncoupling of mitochondria, something that did not happen with SANA. Even more, neither the saturated form of SANA (M1), nor different isomers and analogues

(3-SANA, 4-SANA, E-SANA) had any effect on thermogenesis and expression of creatine markers, supporting that the thermogenic effect of SANA is exclusive of this form of the molecule.

SANA activated several key regulatory genes that have been identified as requisite to boost creatine metabolism in adipose tissue, including different creatine kinases and key enzymes for creatine synthesis. Disruption of creatine metabolism in vivo with the creatine antagonist β -GPA completely abolished the pro-thermogenic effect of the drug (Fig. 5m). Originally, CKMT1 was proposed to drive creatine phosphorylation in beige adipose tissue¹⁹. More recently, the same researchers proposed that CKB controls creatine-dependent thermogenesis in BAT³⁷. However, the role of creatine kinase B (CKB) in mitochondrial creatine metabolism³⁸, and how the creatine-dependent thermogenic cycle works has been questioned^{39,40}. In human adipose cells CKB is exclusively located in the cytosol³⁸, different from mouse adipocytes, where it has been definitively located into the mitochondria³³. This suggests that the pathway is complex, may have species-specific regulation, and needs further investigation. On the other hand, several reports suggest that CKMT2 is an important player in adipose tissue thermogenesis, that is, downregulation of *Ckmt2* in adipose cells decreases phosphocreatine levels³⁸, and silencing of β_3 -adrenergic receptors in beige/brown adipose cells decreases both *Ckmt1* and *Ckmt2* expression⁴¹. Also, bile acids increase mitochondrial function in white adipocytes, stimulating a thermogenic programme that is partially dependent on CKMT2 expression⁴². There is also evidence suggesting that downregulation of *Ckmt2* in skeletal muscle in hibernating bears is linked to metabolic reprogramming involving an increase in glycolysis⁴³. Nevertheless, to date, CKB is the only creatine kinase isoform that has been genetically demonstrated to mediate creatine kinase activity in mouse adipocytes and in mitochondria of thermogenic fat cells^{33,37}.

We found that in iWAT, SANA stimulated both *Ckmt1* and *Ckm* during DIO. However, in BAT, *Ckmt2* and *Ckm* were the main kinases upregulated by SANA. While there is no evidence supporting that *Ckm* participates in creatine-dependent thermogenesis, the differential response among treatments and tissues suggests that there may be some level of redundancy among contributory kinases, as well as differential responses between acute and chronic thermogenic activity. In fact, RNA-sequencing analysis of human adipocyte cells⁴⁴ shows that activation by forskolin promotes an increase in expression of more than one creatine kinase, which is also seen in vivo by cold exposure (Extended Data Fig. 9). Interestingly, an alternative theoretical model for creatine-dependent thermogenesis has been proposed, which resembles its canonical role in skeletal muscle and other tissues of high energy expenditure⁴⁵, as a fast energy provider for Ca^{2+} reuptake into the endoplasmic reticulum³⁹. Under this proposal, two kinases—one mitochondrial and one cytosolic—are necessary. This model better reconciles with our results using SANA, where *Ckm* is systematically upregulated, and does not necessarily antagonize the experimental evidence already published^{19,23,37}. Interestingly, cold exposure promotes an increase in mitochondrial and cytosolic creatine kinases both in iWAT and BAT (Extended Data Fig. 9). Indeed, CKMT1/CKB-double KO mice show defective thermoregulation⁴⁶, further supporting this idea. Nevertheless, recent work shows that TNAP/ALPL is indeed necessary for creatine futile cycle and body temperature maintenance in the absence of UCPI, demonstrating that CKB and TNAP/ALPL are key for the creatine futile cycle in mice during cold exposure³³. These apparent discrepancies could imply that, while promoting creatine-dependent adipose tissue activation and thermogenesis, SANA does not completely phenocopy the pathway activation as during cold exposure. In fact, when we studied cold response in BAT and iWAT in untreated mice, we also found that *Ckb* is upregulated (Extended Data Fig. 9), but despite this creatine kinase is not affected by SANA. It is plausible then, that the pharmacological pathway activated by the drug phenocopies the physiological thermogenic, cold-elicited creatine-dependent thermogenesis, but through activation of different kinases. Our results

show that SANA-induced thermogenesis relies, at least partially, on CKMT1. CKMT1-KO mice had compromised thermoregulatory capacity, but only when treated with SANA, not in basal conditions⁴⁷. Furthermore, when maintained at thermoneutrality, CKMT1-KO mice showed no response to SANA in glucose management. Some of us recently proposed that CKMT1 is dispensable for mitochondrial function in white adipose cells, and CKMT1-KO mice have no alterations in viability, normal development or metabolic parameters, including thermoregulation in normal or HFD feeding⁴⁷. The fact that *Ckmt1*-KO mice have diminished thermoregulatory capacity only when treated with SANA, suggests that CKMT1 plays a role in thermoregulation and that *Ckmt1*-KO mice might develop compensatory mechanisms to cope with this deficiency. It also suggests that treatment with SANA somehow commits mice to creatine-dependent metabolism for thermoregulation, to the detriment of other thermogenic pathways, compromising the flexibility of the thermogenic response. In fact, depletion of creatine in vivo not only abolished the effect of SANA on thermoregulation, but also in some cases seemed to worsen it (Fig. 5m). Experimental evidence suggests the existence of a dynamic cross-talk between UCPI and creatine-dependent thermogenic pathways where they seem to go in opposite directions¹⁹. It is plausible then, that hyperactivation of creatine metabolism in adipose tissue by SANA will impede the activation of UCPI in case of need. Activation of thermogenesis and beigeing of white adipose tissue has been linked to increased mitochondrial biogenesis. Our gene expression, including upregulation of PGC1 α , suggest SANA is promoting mitochondrial biogenesis. Nevertheless, when we measured mitochondrial number in iWAT in response to SANA, we failed to detect any variations. The cold-elicited increase in mitochondrial number in iWAT can be detected after prolonged and continuous challenge⁴⁸, so it is plausible that failure to detect an increase in mitochondrial number is mainly due to technical limitations. These questions remain to be addressed and will deserve future investigation. Also, the molecular target of SANA remains to be determined. Nevertheless, shedding light into this goes beyond the scope of this work and will certainly be part of future research. Importantly, the complete target of established pharmaceutical interventions to diabetes and obesity such as metformin⁴⁹ or to endogenous ligands such as lac-phe⁵⁰ have not been completely elucidated, but do not diminish their important clinical and physiological roles. It is also possible that, by affecting creatine metabolism, other tissues where creatine metabolism is of key importance, such as skeletal muscle, are being altered. Indeed, although we performed several in vivo studies of muscle function and did not see any affection, we did see increased creatine levels in SANA-treated mice. Whether there are alterations in skeletal muscle function that are also contributing to the metabolic effects of SANA cannot be completely ruled out and deserves future investigation. Finally, we evaluated the safety, tolerability, pharmacokinetics and pharmacodynamics of SANA in a randomized, double-blind, placebo-controlled study phase 1A/B, first-in-human clinical trial. In the SAD cohort, SANA was well tolerated up to 400 mg, showing adverse side effects at the highest dose (800 mg). In the MAD cohort (100–200 mg/12 h), SANA showed a favorable safety and tolerability profile for 15 days of treatment, with minor AEs. No moderate or severe gastrointestinal adverse effects were reported (Table 1). Although the aim of the trial was to evaluate the safety of the drug, very importantly, we found a significant decrease in body weight in the highest dose of the MAD cohorts 2 and 3 (100 mg and 200 mg/12 h), while no significant weight loss was measured in the placebo (Fig. 7 and Extended Data Table 1). It is important to highlight that the weight loss of -3% measured in cohort 3 (200 mg/12 h) is very similar to the results obtained with semaglutide in the same time frame². Even more, when metabolic parameters were measured, in cohort 3 (200 mg/12 h) there was a significant improvement in glucose metabolism (HOMA-IR, fructosamine) in volunteers with overweight/obesity, at doses averaging -2 mg per kg per day (Fig. 7). It is worth noting that the improvement in glucose management in the MAD cohort

3 may be greater than expected to the body weight change observed. The possibility that SANA has effects on insulin sensitivity that go beyond the weight-lowering effect will be the subject of further clinical investigation. Also, it is worth mentioning that one of the participants in cohort 3 showed increased basal glycaemia despite showing decreased body weight and insulin levels. All these aspects remain to be studied and warrant a larger clinical trial focused on efficacy. Overall, SANA appears to be safe in humans, showing promising signs of efficacy, supporting the view that it is a good candidate to improve the current therapies for obesity and associated comorbidities.

Limitations of the study

Although the human results obtained during the phase 1A/B clinical trial supports the notion that SANA may be effective in humans, it is important to take into consideration that the clinical trial was designed with the main objective of determining safety and tolerability, with a limited number of volunteers and clinical determinations. In that sense, the efficacy of SANA in humans needs to be further studied in a phase 2 clinical trial, with longer treatment, increased sample number, and extended measurements to validate its efficacy and mechanism of action. As such, the efficacy results presented here, although promising, are still preliminary and subject to further validation.

Conclusion

Non-shivering thermogenesis is a homeostatic response present in mice and humans that can be subject to pharmacological stimulation. Boosting of creatine metabolism and thermogenesis in adipose tissue reveals a promising therapeutic opportunity for the treatment of metabolic diseases. The current study presents compelling preclinical and clinical evidence that SANA is a potent drug for the treatment of DIO, with a primary mechanism of action being the activation of creatine-dependent energy expenditure and thermogenesis in adipose tissue. Importantly, this activation also occurs at thermoneutrality, a condition that reflects everyday human life. This study provides the evidence that boosting creatine metabolism in adipose tissue is an effective pathway to prevent and treat DIO. Importantly, although our human clinical study was designed as a phase 1A/B safety and tolerability study, patients in the MAD cohort receiving the highest dose of SANA not only tolerated it well but also showed significant decrease in body weight and amelioration of glucose management over a 15-day treatment. In summary, we present a comprehensive study of a molecule as a putative treatment for obesity, from the design, characterization, preclinical validation, mechanism of action to a phase 1A/B human clinical study. SANA appears to be a promising, first-in-class small molecule that could have a critical role in the treatment of obesity and metabolic syndrome.

Methods

Reagents and resources

The key reagents and resources are listed in Supplementary Table 1.

Cell lines

TERT-hWA cells were kindly provided by J. B. Hansen⁵¹ and cultured in 10% FBS/Advanced DMEM/F-12 media. Cells were induced to differentiate with insulin (5 µg ml⁻¹), dexamethasone (1 µM), IBMX (0.5 mM), rosiglitazone (1 µM), human cortisol (1 µM) and T3 (1 nM). At day 12 after stimuli, the adipocytes were considered mature. Cell lines were purchased from the American Type Culture Collection (ATCC). THP-1 cells (ATCC, TIB-202) were grown with 10% FBS/RPMI media and differentiated to macrophages with 200 nM PMA for 48 h at 37 °C in 5% CO₂. C2C12 cells (ATCC, CRL-1772) were grown with 10% FBS/DMEM media.

Animals

C57BL/6J (Jackson Labs) mice and zebrafish (*Danio rerio*) were maintained at the Institut Pasteur de Montevideo Animal facility (UBAL). The experimental protocol was approved by the Institutional Animal

Care and Use Committee (IACUC) of the Institut Pasteur de Montevideo (CEUA, protocol nos. 003-19 and 006-19). Studies were performed according to the methods approved in the protocol.

For the CLAMS studies, C57BL/6J mice were purchased from the Jackson Laboratory, and the experiments were approved by the IACUCs of West Virginia University and Mayo Clinic (Jacksonville, USA; IACUC no. A00003888-18-R24).

AMPK, Ckmt1 and UCP1-KO mice were also used. WT and AMPK-KO mice (α1) on a C57BL/6J/129 mixed background were bred and maintained at the Henry Ford Health animal facility as previously described⁵². All experiments were approved by the Animal Care Committee (IACUC, 1530).

Ckmt1-KO and WT mice on a C57BL/6N background were maintained at the University of Guelph as previously described⁴⁷. All experiments were approved by the Animal Care Committee (AUP, 5071) at the University of Guelph and met the guidelines of the Canadian Council on Animal Care.

WT and littermate homozygous UCP1-KO mice on a pure C57BL/6J genetic background were bred and maintained at University of Sao Paulo animal facility. UCP1-KO and WT mice were generated by crossing heterozygous UCP1-KO mice (B6.129-Ucp1tm1Kz/J, Jackson Laboratories) on a C57BL/6J background. All experiments were approved by the Animal Care Committee (CEUA, 6071181120, ICB/USP).

Except where indicated, all the experiments were performed on young male mice (10–12 weeks of age). All animals were housed under a 12-h light–dark cycle. Relative humidity was maintained between 30% and 70%. Food and water were provided ad libitum.

Experiments were conducted at either 22 °C or 28 °C (thermoneutrality) with free access to food and water. Unless specified, mice were housed at 22 °C in groups of five. For thermoneutrality experiments, mice were housed individually at 28 °C (30 °C for UCP1-KO and WT littermate mice) and acclimatized for one week before the start of the experiment.

HFD feeding

Male C57BL/6J, AMPK-KO and CKMT1-KO mice were fed a HFD (42% fat and 0.25% cholesterol, AIN93G, LabDiet), starting at 12 weeks of age and for a duration of 8 weeks for metabolic evaluations. For the reversal of obesity experiments, adult male mice (6 months of age) were fed for 5 weeks with a HFD before the onset of the treatments. UCP1-KO mice were fed for 15 weeks with a high-fat/high-sucrose diet before treatment. Male C57BL/6J mice were also fed a normal diet (46% fat, no cholesterol added, D113, SAFE (https://safe-lab.com/safe_en/), Germany).

Drug delivery

SANA or salicylate (salicylic acid) were administered orally (p.o.) by mixing the drugs as a powder, with the food. Metformin was prepared in a 100 mM phosphate buffer, pH 6.5 and was administered by oral gavage. For s.c. SANA, salicylic acid and M1: 5-(2-nitroethyl)salicylic acid administration, drugs were prepared in a 100 mM phosphate buffer, pH 6.5/PEG 400 (50:50; vol/vol). In all cases the vehicle was used as control.

Cold challenge experiments

C57BL/6J male mice previously acclimatized at 22 °C were treated or not (control) with SANA (or salicylic acid, 20 mg per kg per day, s.c.), in combination or not with β-GPA (0.4 g per kg body weight in PBS pH 7.5, i.p.) for 5 days and fed with normal chow diet. At that point, mice were housed individually at 4 °C from 1–6 h, with free access to food and water. Body temperature was measured before and during the challenge (once every hour) with a mouse rectal probe (ThermoWorks).

Thermal imaging

Thermal images were collected from non-anaesthetized, awake mice with a FLIR E6 thermal imaging camera. Regions of interest from thermal images were selected and quantified using the FLIR Tools software.

Comprehensive Lab Animal Monitoring System

Mice were maintained in the Comprehensive Lab Animal Monitoring System (Columbus Instruments) for 13 days at 28 °C. They were acclimatized for 7 days and fed with normal chow. At that point, SANA administration (20 mg per kg per day, s.c.) was started and repeated for 6 days. On the second day of administration, the normal chow diet was changed to a HFD for the subsequent 4 days. On the last day mice were injected with CL316,243 (1 mg per kg body weight, i.p. in saline solution). In all cases the vehicle was used as control. Oxygen consumption (VO_2), carbon dioxide production (VCO_2) and activity of individual mice were monitored over the total period. VO_2 and VCO_2 values were used to calculate respiratory exchange ratio, and VO_2 and respiratory exchange ratio values were used to determine energy expenditure (kcal h^{-1}) as described previously⁵³.

Body composition

Lean mass and fat mass of individual mice were measured by quantitative nuclear magnetic resonance (NMR) using an EchoMRI analyser.

iWAT mitochondrial enrichment

For each biological replicate, s.c. iWAT from two to three animals (according to body weight) were dissected, pooled and washed in ice-cold homogenization buffer (250 mM sucrose, 10 mM HEPES, 0.1 mM EGTA, pH 7.2). Homogenization buffer was supplemented with 2% BSA during the isolation of fat mitochondria and the procedure was conducted at 4 °C. Tissues were minced on ice and homogenized in homogenization buffer (5 ml per gram of tissue) using a motorized Potter–Elvehjem Teflon pestle. Homogenates were filtered through clean gauze to remove fat particles and centrifuged at 1,000g for 5 min to pellet nuclei and cell debris. The supernatant was transferred to a clean tube and centrifuged at 10,000g for 15 min to pellet crude mitochondria. The mitochondrial pellet was washed three times with 2 ml of homogenization buffer (without BSA) by centrifugation at 10,000g for 10 min and stored at –80 °C until used.

Proteomics analysis

Sample preparation for LC–MS/MS analysis. For proteomics analyses, three biological replicates were used per condition. Protein quantification was performed by densitometry analysis of whole iWAT or iWAT samples enriched in mitochondria separated on 12.5% SDS–PAGE gels and using a low-molecular-weight protein calibration kit (Amersham, GE Healthcare). For mass spectrometry analysis, equal amounts of each protein sample were separated only up to 1 cm into the resolving gel, fixed and stained with Coomassie Blue R-250. In-gel protein digestion and peptide extraction were performed as previously described⁵² with minimal variations. Briefly, the 1-cm bands were excised, and cysteine residues were reduced and alkylated by sequential incubation with 10 mM dithiothreitol and 55 mM iodoacetamide. Tryptic in-gel digestion was performed by overnight incubation at 37 °C with sequencing-grade trypsin (Promega) in a protease:protein ratio of 1:50 (wt/wt). Tryptic peptides were extracted from the gel by adding 60% acetonitrile/0.1% trifluoroacetic acid in two steps of a 1-h incubation at 30 °C. Samples were dried under vacuum and peptides were desalted using ZipTips C18 (Merck Millipore). Eluted peptides were vacuum dried and dissolved with 0.1% formic acid.

LC–MS/MS analysis. Liquid chromatography–tandem mass spectrometry (LC–MS/MS) analysis was performed with an UltiMate 3000 nanoHPLC system (Thermo Fisher Scientific) coupled to a Q Exactive Plus mass spectrometer (Thermo Fisher Scientific). Samples were loaded onto a precolumn (Acclaim PepMap 100, C18, 75 $\mu\text{m} \times 2$ cm, 3- μm particle size) and separated with an Easy-Spray analytical column (PepMap RSLC, C18, 75 $\mu\text{m} \times 50$ cm, 2 μm particle size) at 40 °C using a two-solvent system: (A) 0.1% formic acid in water, (B) 0.1% formic acid in acetonitrile. Separation was achieved through an elution gradient as

follows: 1% to 35% B over 150 min and 35% to 99% B over 20 min, at a flow rate of 200 nL min^{–1}. The mass spectrometer was operated in positive mode using a top 12 data-dependent method. Ion spray voltage was set at 2.5 kV and capillary temperature at 250 °C. The survey scans were acquired in the range of 200–2,000 m/z with a resolution of 70,000 at 200 m/z , an AGC target value of 1×10^6 and a maximum ion injection time of 100 ms. Precursor fragmentation occurred in an HCD cell with a resolution of 17,500 at 200 m/z , an AGC target value of 1×10^4 and a maximum ion injection time of 50 ms. Normalized collision energy was used in steps of 25, 30 and 35. Dynamic exclusion time was set to 30 s. Each sample was injected twice.

Mass spectrometry data analysis. PatternLab for Proteomics v4.1.1.25 (PatternLab)⁵⁴ was used to perform peptide-spectrum matching against a *Mus musculus* proteome from UniProt (UP000000589, downloaded on 26 August 2020) and label-free quantitative analysis. Search results were filtered by the PatternLab Search Engine Processor (SEPro) algorithm with a maximum false discovery rate value $\leq 1\%$ at the protein level and 10 ppm tolerance for precursor ions. PatternLab's Venn diagram statistical module was performed according to a PatternLab Bayesian model to determine proteins uniquely detected in each biological condition using a probability value less than 0.05 (refs. 54,55). PatternLab's TFC module was used to relatively quantify proteins present in both biological conditions by a spectrum count-based label-free quantification method. Proteins present in at least four biological replicates from the total of six were considered for TFC analysis. This module uses the Benjamini–Hochberg's theoretical estimator to deal with multiple t -tests and it maximizes the number of identifications satisfying a fold change cut-off that varies with the P values (Benjamini–Hochberg $q < 0.05$) while restricting false differential proteins mainly due to low abundance⁵⁶. The list of statistically overrepresented proteins in the condition HFD + SANA, obtained from Venn diagram and TFC PatternLab's modules, was subjected to pathway enrichment analysis. The *Mus musculus* total proteome or the mitochondrial proteome obtained in our experiment were used as background proteomes for the over-representation analysis of the total or mitochondrial protein sets, respectively, using the functional enrichment analysis web tool WebGestalt 2019 (ref. 57). The mass spectrometry proteomics data have been deposited in the ProteomeXchange Consortium via the PRIDE⁵⁸ partner repository under dataset identifier PXD030485.

Metabolite analysis by LC–MS/MS and NMR. All NMR experiments were performed on a Bruker AVANCE III 500 NMR spectrometer equipped with a room temperature z-gradient TXI probe and operating at ¹H and ¹³C frequencies of 500.13 MHz and 125.76 MHz, respectively. Water-suppressed ¹H NMR spectra were recorded using a one-dimensional nuclear Overhauser effect spectroscopy (1D-NOESY) pulse sequence with pre-saturation at 25 °C. A spectral width of 10 KHz, a data size of 32,000, and a total of 128 scans with a relaxation delay of 4 s between scans were used to record each experiment. All free induction decays were zero-filled to 64,000 points and apodized with a 0.3-Hz exponential window function before Fourier transformation. Spectra were referenced to the α -glucose anomeric proton resonance at 5.22 ppm present in all samples. Metabolites were identified by comparison to spectra from public databases, assisted with data obtained from standard gradient-enhanced HSQC spectra when necessary. Metabolite concentrations in the NMR sample were estimated using the PULCON method as implemented in the spectrometer and normalized to wet tissue mass to yield concentrations in nanomoles per milligram of tissue. For LC–MS/MS analysis, the extracts were analysed by a Shimadzu LC Nexera X2 UHPLC coupled with a QTRAP 5500 LC–MS/MS (AB Sciex). An ACQUITY UPLC BEH Amide analytic column (2.1 \times 50 mm, 1.7 μm , Waters) was used for chromatographic separation. The extracted multiple reaction monitoring peaks were integrated using MultiQuant 3.0.2 software (AB Sciex).

Respirometry of adipocytes and cells. Oxygen consumption of cultured differentiated adipocytes and iWAT adipocytes was measured with a high-resolution respirometer (Oxygraph-2k, OROBOROS INSTRUMENTS) and Seahorse (Agilent Technologies). Adipocyte suspension was pipetted into 2.2-ml mitochondrial respiration medium (MIRO5). For oxygen consumption measurements of intact adipocytes, pyruvate (5 mM) was injected, and basal cellular respiration was recorded⁵⁹. Proton leak respiration was assessed by addition of oligomycin (2 µg ml⁻¹). Titration of FCCP (0.5-µM steps) was performed for measuring maximal cellular respiration rates. Non-mitochondrial oxygen consumption was determined in the presence of antimycin A (0.5 µM) and rotenone (0.5 µM). Adipocyte respiration measurements were normalized by the µg ml⁻¹ of DNA. Basal respiration was determined before the addition of inhibitors and the uncoupler. Oligomycin-resistant and oligomycin-sensitive respiration rates were the ATP-independent (leak) and ATP-dependent respiration rates, respectively. Maximum respiration rate was obtained after titration with FCCP, and the spare respiratory capacity was the difference between the maximum and basal respiration⁶⁰. Mito-Stress Test assays were performed using the Seahorse XFe96 Bioanalyzer and Seahorse 96-well XF cell culture microplates according to manufacturer's instructions.

RNA isolation and real-time RT-qPCR. Total RNA was isolated from cells or tissues using TRIzol Reagent and the Direct-zol RNA MiniPrep kit (Zymo Research) according to the manufacturer's instructions. All primers were synthesized by Integrated DNA Technology. The complete list of primers and the number of samples used for each gene analysed in mice are shown in Supplementary Table 1.

Clinical study. Participants. This was a phase 1, first-in-human, single- and multiple-dose escalation clinical study, conducted in normal weight or healthy adult volunteers with overweight or obesity, performed at CMAX Clinical Research Facility, Adelaide, Australia. The safety, tolerability, pharmacokinetics and pharmacodynamics of MVD1 following single- and multiple-dose administrations was evaluated using a randomized, double-blind, placebo-controlled study design. Forty-one adult volunteers (aged 18–60 years, body mass index BMI 20–30 kg/m² for SAD and aged 25–60 years, BMI 28–35 kg/m²) were recruited from the general population in the vicinity of Adelaide, Australia, through advertisements. The clinical study was performed in accordance with the World Medical Association Declaration of Helsinki, the International Council for Harmonisation of Technical Requirements for Pharmaceuticals for Human Use (ICH) Guideline for Good Clinical Practice (GCP) E6 (R2), the applicable regulatory requirements, and the Australian National Health and Medical Research Council National Statement on Ethical Conduct in Human Research incorporating all updates. Trial registration and details can be found at the Australian New Zealand Clinical Trials Registry (<https://www.anzctr.org.au/>, registration number: ACTRN12622001519741, date submitted: 21 November 2022, date registered: 7 December 2022, last update: 11 August 2024, secondary ID: MVD1-AU-001). The Bellberry Human Research Ethics Committee reviewed this study in accordance with the National Health and Medical Research Council's National Statement on Ethical Conduct in Human Research (2007, incorporating all updates) on the above meeting date. The principal investigator and co-investigators were not members of the Bellberry Human Research Ethics Committee that reviewed this study. All participants provided written informed consent.

Primary, secondary and exploratory endpoints. *Primary endpoints.* Safety endpoints included the evaluation of the change from baseline and, where appropriate, over time and versus placebo, including: (1) Incidence, severity, and relationship of AEs or serious AEs (including withdrawals due to AEs). (2) Change in vital signs. (3) Change in electrocardiogram parameters. (4) Change in clinical laboratory parameters

(haematology, serum chemistry, coagulation and urinalysis). (5) Stool diary. (6) Nutritional appetite questionnaire (part B only).

Secondary endpoints. Plasma MVD1 and metabolite M1 pharmacokinetic endpoints included: (1) Maximum observed plasma concentration (C_{max}). (2) Time to C_{max} (T_{max}). (3) Area under the plasma concentration–time curve from time 0 to time of last quantifiable concentration (AUC_{0-last}). (4) Area under the plasma concentration–time curve from time 0 extrapolated to infinity (AUC_{0-inf}) following a single dose only. (5) Apparent terminal elimination half-life ($t_{1/2}$). (6) Terminal elimination rate constant (λ_z). (7) Apparent clearance (CL/F). (8) Apparent volume of distribution (V_z/F ; part A only). (9) Minimum observed concentration C_{min} (day 15; part B only). (10) Area under the plasma concentration–time curve from time 0 to 12 h (AUC_{0-12}). Urine MVD1 pharmacokinetic endpoints included (but were not limited to): (1) Cumulative amount of unchanged drug excreted (A_e) in urine. (2) Renal clearance (CL_r)

Exploratory endpoints (MAD only). Exploratory endpoints included: (1) Body weight (day –1, day 15 and day 22); (2) glucose; (3) insulin; (4) fructosamine; (5) the Patient Global Impression of Change (PGIC) questionnaire completed by study participants at the end of the study treatment period.

Part A (SAD) consisted of three cohorts (S1–S3) with six participants planned per cohort, randomized at a ratio of 2:1 (MVD1:placebo) within each cohort. Participants were dosed once a day via the oral route of administration. Dose escalation was planned for part A (SAD; 200, 400 or 800 mg per dose). Participants eligible for inclusion in the study were admitted to the investigational site on day –1. Following confirmation of eligibility on day 1, participants were enrolled and randomized to receive either MVD1 or placebo. Dosing occurred on day 1 with MVD1 or placebo in a double-blind manner. Participants were discharged from the clinical facility on day 4 following completion of study assessments and were required to attend the clinic for a final follow-up visit on day 8 ± 1 day. For each part A cohort, dosing was initiated in two sentinel participants with one participant randomized to receive MVD1 and the other randomized to receive placebo. The remainder of the participants within each cohort only commenced dosing following satisfactory review of sentinel day 2 data by the principal investigator/independent medical monitor. Escalation to the next dose level occurred following satisfactory Safety Review Committee review of available safety data up to day 4 and available pharmacokinetic data from all participants at that dose level.

Part B (MAD) consisted of three cohorts (M1–M3) with eight participants planned per cohort, randomized at a ratio of 3:1 (MVD1:placebo) within each cohort. Healthy adult volunteers with overweight or obesity were screened between day –35 and day –2, inclusive. Participants eligible for inclusion in the study were admitted to the investigational site on day –1. Following confirmation of eligibility on day 1, participants were enrolled and randomized to receive either MVD1 or placebo. Dosing occurred on days 1 to 15 with MVD1 or placebo (two daily oral doses of study drug taken 12 h apart (morning and evening) on days 1–14 with a final single-dose administration on the morning of day 15) in a double-blind manner. Participants were discharged from the clinical facility on day 18 following completion of study assessments and were required to attend the clinic for a final follow-up visit on day 22 ± 1 day. Body weight was measured on days 1, 15 and 22. Blood samples for pharmacokinetic and pharmacodynamic analysis were to be collected before the dose and at several time points after the dose. MAD was conducted as an inpatient study. Participants were dosed twice a day (administered approximately 12 h apart, one in the morning and one in the evening) for 14 days, with a single dose administered on day 15 via the oral route. All the meals were provided at the facility and including at least 250–300 g of carbohydrates per day. At the end of the 15-day period, patients were asked to fulfil a quality questionnaire (PGIC) regarding appetite and satiety. There were no reports of affectation of

appetite or satiety by the tested volunteers. Participants were required to fast overnight for at least 8 h before the screening visit and before admission to the clinical facility on day −1. On all dosing days (day 1 to day 15), participants were required to fast for at least 2 h before administration of each dose of study drug and until at least 2 h after dose. A final overnight fast of at least 8 h was required on day 15 before final pharmacodynamic measurements on day 16. During all fasting periods in part A (SAD) and part B (MAD), no food or beverages were to be consumed by the study participants except for water.

Alterations of the original protocol. In the SAD cohort 3, the last patient was not dosed. The Safety Review Committee decided the dose at the no-observed-adverse-effect level was already determined and recommended to end the SAD arm of the study. In the MAD cohort, one volunteer was excluded from the trial due to a protocol deviation in the inclusion criteria (age mismatch with MAD inclusion criteria). It was later determined that the volunteer was randomized as a placebo. In MAD cohort 1 (100 mg/12 h), one participant was withdrawn from the study, following the advice of the Safety Review Committee, due to an event of proteinuria deemed mild and unrelated to study treatment, and most probably related to a pre-existing renal disease that was not detected during the screening period. Due to an error in the original protocol, which was later amended, body weight could not be determined for two placebo and four treated volunteers in cohort 1.

HOMA-IR calculations

Fasting glucose and fasting insulin were measured from the same blood sample and the values obtained were used to calculate HOMA-IR using the following formula: $\text{HOMA-IR} = (\text{insulin (mU l}^{-1}) \times \text{glucose (mg dl}^{-1}) / 405$.

Statistical analysis

No statistical methods were used to predetermine sample sizes, but our sample sizes are similar to those reported in previous publications^{19,23,61,62}. For in vivo studies, mice were randomly assigned to treatment groups. For clinical studies, double blinding and randomization were performed by a third party. Samples were processed in random order. Data collection and analysis were not performed blind to the conditions of the experiments. Results are presented as the mean \pm s.e.m. of biologically independent samples. In cases where independent data were pooled, the approach is disclosed in the corresponding figure legend. Data were tested for normality using D'Agostino & Pearson or Shapiro–Wilk tests, and equal variances were analysed using the Levene test, meeting the assumptions of the statistical tests used. Paired and unpaired two-sided Student's *t*-test for pairwise comparison, one-way ANOVA followed by Bonferroni post hoc for multiple comparisons, two-way ANOVA followed by Tukey's multiple-comparisons test, linear regression and ANCOVA for in vivo metabolic analyses and log-rank (Mantel–Cox) test for Kaplan–Meier curve comparisons were used to calculate *P* values. Bayesian framework with a Poisson distribution and multiple unpaired Student's *t*-tests (one per protein) with Benjamini–Hochberg correction for multiple comparisons in proteomics analyses were used. In all cases $P < 0.05$ was considered statistically significant. No animals or data points were excluded from the analyses. Calculations were done using GraphPad Prism and Jasp (JASP Team, 2024, version 0.19.2).

Reporting summary

Further information on research design is available in the Nature Portfolio Reporting Summary linked to this article.

Data availability

For proteomic analysis, the *Mus musculus* proteome from UniProt (UP000000589) was used. The mass spectrometry proteomics data have been deposited to the ProteomeXchange Consortium via the

PRIDE partner repository under dataset identifier PXD030485 (<https://www.ebi.ac.uk/pride/archive/projects/PXD030485>). Clinical trial registration and details can be found at the Australian New Zealand Clinical Trials Registry (<https://www.anzctr.org.au/>; registration: ACTRN12622001519741). Source data are provided with this paper. All the remaining data that support the plots are available as part of the Supplementary Information, and all the experimental protocols that support the findings of this study are available from the corresponding authors upon request.

References

1. Flegal, K. M., Graubard, B. I., Williamson, D. F. & Gail, M. H. Cause-specific excess deaths associated with underweight, overweight, and obesity. *JAMA* **298**, 2028–2037 (2007).
2. Wilding, J. P. H. et al. Once-weekly semaglutide in adults with overweight or obesity. *N. Engl. J. Med.* **384**, 989–1002 (2021).
3. Villacorta, L., Gao, Z., Schopfer, F. J., Freeman, B. A. & Chen, Y. E. Nitro-fatty acids in cardiovascular regulation and diseases: characteristics and molecular mechanisms. *Front. Biosci.* **21**, 873–889 (2016).
4. Batthyany, C. et al. Reversible post-translational modification of proteins by nitrated fatty acids in vivo. *J. Biol. Chem.* **281**, 20450–20463 (2006).
5. Kelley, E. E. et al. Fatty acid nitroalkenes ameliorate glucose intolerance and pulmonary hypertension in high-fat diet-induced obesity. *Cardiovasc. Res.* **101**, 352–363 (2014).
6. Rom, O. et al. Nitro-fatty acids protect against steatosis and fibrosis during development of nonalcoholic fatty liver disease in mice. *EBioMedicine* **41**, 62–72 (2019).
7. Ibarburu, S. et al. A nitroalkene benzoic acid derivative targets reactive microglia and prolongs survival in an inherited model of ALS via NF-kappaB inhibition. *Neurotherapeutics* **18**, 309–325 (2021).
8. Dapuerto, R. et al. A novel nitroalkene vitamin E analogue inhibits the NLRP3 inflammasome and protects against inflammation and glucose intolerance triggered by obesity. *Redox Biol.* **39**, 101833 (2021).
9. Rodriguez-Duarte, J. et al. A novel nitroalkene- α -tocopherol analogue inhibits inflammation and ameliorates atherosclerosis in Apo E knockout mice. *Br. J. Pharmacol.* **176**, 757–772 (2019).
10. Rodriguez-Duarte, J. et al. Electrophilic nitroalkene-tocopherol derivatives: synthesis, physicochemical characterization and evaluation of anti-inflammatory signaling responses. *Sci. Rep.* **8**, 12784 (2018).
11. Jack, D. B. One hundred years of aspirin. *Lancet* **350**, 437–439 (1997).
12. van Dam, A. D. et al. Salsalate activates brown adipose tissue in mice. *Diabetes* **64**, 1544–1554 (2015).
13. Smith, B. K. et al. Salsalate (salicylate) uncouples mitochondria, improves glucose homeostasis, and reduces liver lipids independent of AMPK- β 1. *Diabetes* **65**, 3352–3361 (2016).
14. Nie, L. et al. Salsalate activates skeletal muscle thermogenesis and protects mice from high-fat diet induced metabolic dysfunction. *EBioMedicine* **23**, 136–145 (2017).
15. Hawley, S. A. et al. The ancient drug salicylate directly activates AMP-activated protein kinase. *Science* **336**, 918–922 (2012).
16. Goldfine, A. B. et al. The effects of salsalate on glycemic control in patients with type 2 diabetes: a randomized trial. *Ann. Intern. Med.* **152**, 346–357 (2010).
17. Goldfine, A. B. et al. Salicylate (salsalate) in patients with type 2 diabetes: a randomized trial. *Ann. Intern. Med.* **159**, 1–12 (2013).
18. Salastekar, N. et al. Salsalate improves glycaemia in overweight persons with diabetes risk factors of stable statin-treated cardiovascular disease: a 30-month randomized placebo-controlled trial. *Diabetes Obes. Metab.* **19**, 1458–1462 (2017).

19. Kazak, L. et al. A creatine-driven substrate cycle enhances energy expenditure and thermogenesis in beige fat. *Cell* **163**, 643–655 (2015).
20. De Meis, L., Ketzer, L. A., Camacho-Pereira, J. & Galina, A. Brown adipose tissue mitochondria: modulation by GDP and fatty acids depends on the respiratory substrates. *Biosci. Rep.* **32**, 53–59 (2012).
21. Oudman, I., Clark, J. F. & Brewster, L. M. The effect of the creatine analogue beta-guanidinopropionic acid on energy metabolism: a systematic review. *PLoS ONE* **8**, e52879 (2013).
22. Kazak, L. et al. Genetic depletion of adipocyte creatine metabolism inhibits diet-induced thermogenesis and drives obesity. *Cell Metab.* **26**, 660–671 (2017).
23. Kazak, L. et al. Ablation of adipocyte creatine transport impairs thermogenesis and causes diet-induced obesity. *Nat. Metab.* **1**, 360–370 (2019).
24. Rubino, D. M. et al. Effect of weekly subcutaneous semaglutide vs daily liraglutide on body weight in adults with overweight or obesity without diabetes: the STEP 8 randomized clinical trial. *JAMA* **327**, 138–150 (2022).
25. Sodhi, M., Rezaeianzadeh, R., Kezouh, A. & Etminan, M. Risk of gastrointestinal adverse events associated with glucagon-like peptide-1 receptor agonists for weight loss. *JAMA* **330**, 1795–1797 (2023).
26. Lenharo, M. Anti-obesity drugs' side effects: what we know so far. *Nature* **622**, 682 (2023).
27. Hussain, M. F., Roesler, A. & Kazak, L. Regulation of adipocyte thermogenesis: mechanisms controlling obesity. *FEBS J.* **287**, 3370–3385 (2020).
28. Cypess, A. M. et al. Identification and importance of brown adipose tissue in adult humans. *N. Engl. J. Med.* **360**, 1509–1517 (2009).
29. Hanssen, M. J. et al. Short-term cold acclimation recruits brown adipose tissue in obese humans. *Diabetes* **65**, 1179–1189 (2016).
30. Roesler, A. & Kazak, L. UCP1-independent thermogenesis. *Biochem. J.* **477**, 709–725 (2020).
31. Kazak, L. & Spiegelman, B. M. Mechanism of futile creatine cycling in thermogenesis. *Am. J. Physiol. Endocrinol. Metab.* **319**, E947–E949 (2020).
32. Rahbani, J. F. et al. Parallel control of cold-triggered adipocyte thermogenesis by UCP1 and CKB. *Cell Metab.* <https://doi.org/10.1016/j.cmet.2024.01.001> (2024).
33. Bunk, J. et al. The Futile Creatine Cycle powers UCP1-independent thermogenesis in classical BAT. *Nat. Commun.* <https://doi.org/10.1038/s41467-025-58294-4> (2025).
34. Vargas-Castillo, A. et al. Development of a functional beige fat cell line uncovers independent subclasses of cells expressing UCP1 and the futile creatine cycle. *Cell Metab.* <https://doi.org/10.1016/j.cmet.2024.07.002> (2024).
35. Wang, T. et al. Single-nucleus transcriptomics identifies separate classes of UCP1 and futile cycle adipocytes. *Cell Metab.* <https://doi.org/10.1016/j.cmet.2024.07.005> (2024).
36. Meex, R. C., Phielix, E., Moonen-Kornips, E., Schrauwen, P. & Hesselink, M. K. Stimulation of human whole-body energy expenditure by salsalate is fueled by higher lipid oxidation under fasting conditions and by higher oxidative glucose disposal under insulin-stimulated conditions. *J. Clin. Endocrinol. Metab.* **96**, 1415–1423 (2011).
37. Rahbani, J. F. et al. Creatine kinase B controls futile creatine cycling in thermogenic fat. *Nature* **590**, 480–485 (2021).
38. Maqdasy, S. et al. Impaired phosphocreatine metabolism in white adipocytes promotes inflammation. *Nat. Metab.* **4**, 190–202 (2022).
39. Wallimann, T., Tokarska-Schlattner, M., Kay, L. & Schlattner, U. Role of creatine and creatine kinase in UCP1-independent adipocyte thermogenesis. *Am. J. Physiol. Endocrinol. Metab.* **319**, E944–E946 (2020).
40. Nicholls, D. G. & Brand, M. D. A critical assessment of the role of creatine in brown adipose tissue thermogenesis. *Nat. Metab.* **5**, 21–28 (2023).
41. Cero, C. et al. β 3-Adrenergic receptors regulate human brown/beige adipocyte lipolysis and thermogenesis. *JCI Insight* **6**, e139160 (2021).
42. Wu, Q. et al. Intestinal hypoxia-inducible factor 2 α regulates lactate levels to shape the gut microbiome and alter thermogenesis. *Cell Metab.* **33**, 1988–2003 (2021).
43. Chazarin, B. et al. Metabolic reprogramming involving glycolysis in the hibernating brown bear skeletal muscle. *Front Zool.* **16**, 12 (2019).
44. Min, S. Y. et al. Diverse repertoire of human adipocyte subtypes develops from transcriptionally distinct mesenchymal progenitor cells. *Proc. Natl Acad. Sci. USA* **116**, 17970–17979 (2019).
45. Wallimann, T., Tokarska-Schlattner, M. & Schlattner, U. The creatine kinase system and pleiotropic effects of creatine. *Amino Acids* **40**, 1271–1296 (2011).
46. Streijger, F. et al. Mice lacking brain-type creatine kinase activity show defective thermoregulation. *Physiol. Behav.* **97**, 76–86 (2009).
47. Politis-Barber, V. et al. *Ckmt1* is dispensable for mitochondrial bioenergetics within white/beige adipose tissue. *Function* **3**, zqac037 (2022).
48. Ito, R. et al. Mitochondrial biogenesis in white adipose tissue mediated by JMJD1A–PGC-1 axis limits age-related metabolic disease. *iScience* **27**, 109398 (2024).
49. LaMoia, T. E. & Shulman, G. I. Cellular and molecular mechanisms of metformin action. *Endocr. Rev.* **42**, 77–96 (2021).
50. Li, V. L. et al. An exercise-inducible metabolite that suppresses feeding and obesity. *Nature* **606**, 785–790 (2022).
51. Markussen, L. K. et al. Characterization of immortalized human brown and white pre-adipocyte cell models from a single donor. *PLoS ONE* **12**, e0185624 (2017).
52. Nath, N. et al. Loss of AMPK exacerbates experimental autoimmune encephalomyelitis disease severity. *Biochem. Biophys. Res. Commun.* **386**, 16–20 (2009).
53. Fischer, A. W., Cannon, B. & Nedergaard, J. Optimal housing temperatures for mice to mimic the thermal environment of humans: an experimental study. *Mol. Metab.* **7**, 161–170 (2018).
54. Carvalho, P. C. et al. Integrated analysis of shotgun proteomic data with PatternLab for proteomics 4.0. *Nat. Protoc.* **11**, 102–117 (2016).
55. Carvalho, P. C. et al. Analyzing marginal cases in differential shotgun proteomics. *Bioinformatics* **27**, 275–276 (2010).
56. Carvalho, P. C., Yates, J. R. 3rd & Barbosa, V. C. Improving the TFC test for differential shotgun proteomics. *Bioinformatics* **28**, 1652–1654 (2012).
57. Liao, Y., Wang, J., Jaehnig, E. J., Shi, Z. & Zhang, B. WebGestalt 2019: gene set analysis toolkit with revamped UIs and APIs. *Nucleic Acids Res.* **47**, W199–W205 (2019).
58. Perez-Riverol, Y. et al. The PRIDE database and related tools and resources in 2019: improving support for quantification data. *Nucleic Acids Res.* **47**, D442–D450 (2019).
59. Schottl, T., Kappler, L., Braun, K., Fromme, T. & Klingenspor, M. Limited mitochondrial capacity of visceral versus subcutaneous white adipocytes in male C57BL/6N mice. *Endocrinology* **156**, 923–933 (2015).
60. Brand, M. D. & Nicholls, D. G. Assessing mitochondrial dysfunction in cells. *Biochem. J.* **435**, 297–312 (2011).
61. Escande, C. et al. Deleted in breast cancer 1 limits adipose tissue fat accumulation and plays a key role in the development of metabolic syndrome phenotype. *Diabetes* **64**, 12–22 (2015).
62. Bresque, M. et al. SIRT6 stabilization and cytoplasmic localization in macrophages regulates acute and chronic inflammation in mice. *J. Biol. Chem.* **298**, 101711 (2022).

Acknowledgements

C.E. was supported by grants by ANII (ART_X_2023_1_175670, ART_X_2021_1_170221, IDI_X_2023_1_179312 and HPI_X_2024_1_181183), CSIC (22620220100034UD), PEDECIBA and FOCEM (COF 03/11). E.N.C. was supported in part by grants from the the Glenn Foundation for Medical Research via the Paul F. Glenn Laboratories for the Biology of Aging, the Kogod Center on Aging, and NIH National Institute on Aging grants AG26094, AG58812 and CA233790. J.M.H. thanks the support of The National Heart, Lung, and Blood institute (R01 HL-128485 and R01 HL-168290) and the Community Foundation for the Ohio Valley Whipkey Trust. E.E.K. was supported by the National Institutes of Health (NIH; R01 DK124510-01 and R01 HL153532) and the American Heart Association (19TPA34850089). R.R. was supported by Universidad de la República (Espacio Interdisciplinario) and CSIC. M.A.M. was supported by Fundação de Amparo à Pesquisa do Estado de São Paulo (2021/08354-2). R.L. was supported by NIH (R35GM119528). C.E. and R. Daputo thank L. Reyes and CUDIM for technical assistance. W.T.F. was supported by a grant from FAPESP (2020/04159-8). S.G. is supported by the NIH (NS112727 and AI144004). We thank A. P. Arévalo and the rest of the personnel at the Animal Facility (UBAL) at the Institut Pasteur Montevideo for technical assistance with X-ray images and animal care, and A. B. Stewart, Animal Models, and Imaging Facility, WVU, for technical assistance, and Mega Labs S.A. and M. Giusti for providing metformin. A. Leyva, L.C. and M.B. were supported by scholarships from ANII (POS_NAC_2015_1_109491, POS_NAC_2016_1_129896 and POS_NAC_2015_1_109950, respectively). M.B., G.A. and C.V. were supported by CAP (Udelar). G.G. was supported by PROINBIO.

Author contributions

Conceptualization, C.E., C.B. and G.V.L.; Methodology, C.E., C.B., G.V.L., E.N.C., M.P.G., E.E.K., A.K. and W.P.; Validation, C.E.; Formal analysis, A. Leyva, R. Durán, K.C. and C.E.; Investigation, K.C., A. Leyva, J.R.-D., A.B.-R., V.P.-T., S.R., L.C., M.I., L.S., C.V., G.G., L.Z., M.B., R.M.H., R.K., L.M., J.M.A., C. Espasandín, V.d.I.S., R. Daputo, T.R.P., A. Lopez, K.L.T., C.A.L., J.V.F., T.S.V., R. Rattan, G.A., E.D., E.M., S.E.L., G.C.S.B., L.O.L.S., M.S.C., J.C.-P., V.V., A.A., P.C., M.H.V., S.J., A.K., A.C., J.D., Y.W., T.A.W., J.H., S.G., W.T.F., L.O.L. and R.L.; Resources, P.B., J.M.V., J.M.H., R.R., G.M., C.Q., P.M.-V., G.P.H., R.L., E.E.K., R. Durán, M.A.M., W.T.F., L.O.L. and E.N.C.; Data curation, K.C., A. Leyva, R. Durán and T.A.W.; Writing—original draft, C.E., C.B. and G.V.L.; Writing—review and editing, C.E., C.B., G.V.L., E.N.C., E.E.K., R.O.D., K.C., G.P.H. and M.A.M.; Visualization, C.E., K.C., A. Leyva, J.R.-D. and S.R.; Supervision, C.E., M.P.G. and C.B.; Project administration, C.E., C.B., G.V.L., M.P.G. and K.C.; Funding acquisition, C.E., C.B., G.V.L., E.N.C., R. Durán, E.E.K., C.Q. and G.M.

Competing interests

G.V.L., C.B., M.P.G. and C.E. hold shares in EOLO USA Inc. E.N.C. acts as a scientific advisor for EOLO USA Inc. K.C., M.P.G., V.P.-T., M.B., L.S., J.H. and M.I. are used by EOLO USA Inc. The remaining authors declare no competing interests.

Additional information

Extended data is available for this paper at <https://doi.org/10.1038/s42255-025-01311-z>.

Supplementary information The online version contains supplementary material available at <https://doi.org/10.1038/s42255-025-01311-z>.

Correspondence and requests for materials should be addressed to Eduardo N. Chini, Carlos Batthyány or Carlos Escande.

Peer review information *Nature Metabolism* thanks Uwe Schlattner and the other, anonymous, reviewer(s) for their contribution to the peer review of this work. Primary Handling Editors: Revati Dewal, Christoph Schmitt and Isabella Samuelson, in collaboration with the *Nature Metabolism* team.

Reprints and permissions information is available at www.nature.com/reprints.

Publisher's note Springer Nature remains neutral with regard to jurisdictional claims in published maps and institutional affiliations.

Open Access This article is licensed under a Creative Commons Attribution-NonCommercial-NoDerivatives 4.0 International License, which permits any non-commercial use, sharing, distribution and reproduction in any medium or format, as long as you give appropriate credit to the original author(s) and the source, provide a link to the Creative Commons licence, and indicate if you modified the licensed material. You do not have permission under this licence to share adapted material derived from this article or parts of it. The images or other third party material in this article are included in the article's Creative Commons licence, unless indicated otherwise in a credit line to the material. If material is not included in the article's Creative Commons licence and your intended use is not permitted by statutory regulation or exceeds the permitted use, you will need to obtain permission directly from the copyright holder. To view a copy of this licence, visit <http://creativecommons.org/licenses/by-nc-nd/4.0/>.

© The Author(s) 2025

Karina Cal^{1,2,3,48}, Alejandro Leyva^{4,5,48}, Jorge Rodríguez-Duarte^{1,4}, Santiago Ruiz¹, Leonardo Santos^{1,3}, Maria Pia Garat^{1,3}, Lucía Colella^{4,6}, Mariana Ingold^{3,4,6}, Andrés Benitez-Rosendo^{1,2,7}, Valentina Pérez-Torrado^{1,3}, Cecilia Vilaseca⁸, German Galliussi^{4,9}, Lucía Ziegler¹⁰, Thais R. Peclat^{7,11,12}, Mariana Bresque^{1,3}, Rachel M. Handy¹³, Rachel King¹⁴, Larissa Menezes dos Reis^{15,16,17,18}, João Manoel Alves¹⁹, Camila Espasandín^{1,20}, Victoria de la Sovera^{4,6}, Peter Breining²¹, Rosina Daputo^{1,4,22}, Andrés Lopez²³, Katie L. Thompson^{7,11,12}, Caroline A. Lino²⁴, Julia V. França²⁴, Thayna S. Vieira²⁴, Ramandeep Rattan²⁵, Guillermo Agorrodoy²⁶, Evan DeVallance²⁷, Jacqueline Haag³, Ethan Meadows²⁸, Sara E. Lewis^{27,28,29}, Gabriele Catarine Santana Barbosa³⁰, Leonardo Osbourne Lai de Souza³⁰, Marina Santos Chichierchio³⁰, Valeria Valez^{31,32,33}, Adrián Aicardo^{32,33,34}, Paola Contreras^{1,8}, Mikkel H. Vendelbo^{21,35}, Steen Jakobsen³⁵, Andrés Kamaid^{4,5,36}, Williams Porcal^{4,6}, Aldo Calliari^{1,2}, José Manuel Verdes³⁷, Jianhai Du^{28,38}, Yekai Wang³⁸, John M. Hollander^{28,39}, Thomas A. White⁷, Rafael Radi^{32,33}, Guillermo Moyna²³, Celia Quijano^{32,33}, Robert O'Doherty^{40,41}, Pedro Moraes-Vieira^{15,16,17,18}, Shailendra Giri⁴², Graham P. Holloway¹³, William T. Festuccia²⁴, Luiz Osório Leiria¹⁹, Roberta Leonardi^{14,28}, Marcelo A. Mori^{43,44,45,46}, Juliana Camacho-Pereira³⁰, Eric E. Kelley^{27,28,29}, Rosario Duran⁵, Gloria V. López^{4,6}, Eduardo N. Chini^{7,11,12,47}✉, Carlos Batthyány⁴✉ & Carlos Escande¹✉

¹Laboratory of Metabolic Diseases and Aging, Institut Pasteur Montevideo, Montevideo, Uruguay. ²Unidad Biofísica, Departamento de Biociencias, Facultad de Veterinaria, Udelar, Montevideo, Uruguay. ³Eolo USA, Wilmington, DE, USA. ⁴Laboratory of Vascular Biology and Drug Development, Institut Pasteur Montevideo, Montevideo, Uruguay. ⁵Unidad de Bioquímica y Proteómica Analíticas, Institut Pasteur Montevideo and IIBCE, Montevideo, Uruguay. ⁶Departamento de Química Orgánica, Facultad de Química, Udelar, Montevideo, Uruguay. ⁷Robert and Arlene Kogod Center on Aging, Mayo Clinic, Jacksonville, FL, USA. ⁸Departamento de Fisiología, Facultad de Medicina, Udelar, Montevideo, Uruguay. ⁹Laboratory of Immunoregulation and Inflammation; Institut Pasteur Montevideo, Montevideo, Uruguay. ¹⁰Departamento de Ecología y Gestión Ambiental, Centro Universitario Regional del Este, Udelar, Maldonado, Uruguay. ¹¹Department of Anesthesiology, Mayo Clinic, Jacksonville, FL, USA. ¹²Department of Physiology and Biomedical Engineering; Mayo Clinic, Jacksonville, FL, USA. ¹³Department of Human Health and Nutritional Sciences, University of Guelph, Ontario, Canada. ¹⁴Department of Biochemistry and Molecular Medicine, West Virginia University, Morgantown, WV, USA. ¹⁵Laboratory of Immunometabolism, Department of Genetics, Evolution, Microbiology, and Immunology, Institute of Biology, University of Campinas, Campinas, Brazil. ¹⁶Department of Immunology, Institute of Biomedical Sciences, University of São Paulo, São Paulo, Brazil. ¹⁷Obesity and Comorbidities Research Center (OCRC), University of Campinas, Campinas, Brazil. ¹⁸Experimental Medicine Research Cluster (EMRC), University of Campinas, Campinas, Brazil. ¹⁹Department of Pharmacology, Ribeirão Preto Medical School; Department of Cell Biology, Ribeirão Preto Medical School; and Center for Research in Inflammatory Diseases, Ribeirão Preto Medical School, University of São Paulo, Ribeirão Preto, Brazil. ²⁰Unidad Bioquímica, Departamento de Biociencias, Facultad de Veterinaria, Udelar, Montevideo, Uruguay. ²¹Department of Biomedicine, Aarhus University, Aarhus, Denmark. ²²Área I+D Biomédico, CUDIM, Montevideo, Uruguay. ²³Laboratorio de Fisiocoquímica Orgánica, Departamento de Química del Litoral, CENUR Litoral Norte, Udelar, Paysandú, Uruguay. ²⁴Institute of Biomedical Sciences, University of São Paulo, São Paulo, Brazil. ²⁵Division of Gynecology Oncology, Department of Women's Health Services, Henry Ford Health, Detroit, MI, USA. ²⁶Departamento de Fisiopatología, Hospital de Clínicas, Facultad de Medicina, Udelar, Montevideo, Uruguay. ²⁷Department of Physiology and Pharmacology, West Virginia University, Morgantown, WV, USA. ²⁸Mitochondria, Metabolism and Bioenergetics Working Group; School of Medicine, West Virginia University, Morgantown, WV, USA. ²⁹Center for Inhalation Toxicology (iTOX), School of Medicine, West Virginia University, Morgantown, WV, USA. ³⁰Program in Cellular Biochemistry and Biophysics, Institute of Medical Biochemistry Leopoldo de Meis, Federal University of Rio de Janeiro, Rio de Janeiro, Brazil. ³¹Cátedra de Bioquímica y Biofísica, Facultad de Odontología, Udelar, Montevideo, Uruguay. ³²Centro de Investigaciones Biomédicas (CEINBIO), Udelar, Montevideo, Uruguay. ³³Departamento de Bioquímica, Facultad de Medicina, Udelar, Montevideo, Uruguay. ³⁴Departamento de Nutrición Clínica, Escuela de Nutrición, Udelar, Montevideo, Uruguay. ³⁵Department of Nuclear Medicine and PET, Aarhus University Hospital, Aarhus, Denmark. ³⁶Unidad de Bioimagenología Avanzada. Institut Pasteur Montevideo, Montevideo, Uruguay. ³⁷Unidad Patología, Departamento de Patobiología, Facultad de Veterinaria, Udelar, Montevideo, Uruguay. ³⁸Department of Ophthalmology and Visual Sciences, Department of Biochemistry, West Virginia University, Morgantown, WV, USA. ³⁹Division of Exercise Physiology, West Virginia University, Morgantown, WV, USA. ⁴⁰Department of Medicine, Division of Endocrinology and Metabolism, University of Pittsburgh, Pittsburgh, PA, USA. ⁴¹Department of Microbiology and Molecular Genetics, University of Pittsburgh, Pittsburgh, PA, USA. ⁴²Department of Neurology, Henry Ford Health, Detroit, MI, USA. ⁴³Department of Biochemistry and Tissue Biology, Institute of Biology, University of Campinas, Campinas, Brazil. ⁴⁴Obesity and Comorbidities Research Center (OCRC), Campinas, Brazil. ⁴⁵Experimental Medicine Research Cluster (EMRC), Campinas, Brazil. ⁴⁶Instituto Nacional de Obesidade e Diabetes, Campinas, Brazil. ⁴⁷Department of Anesthesiology and Perioperative Medicine, Mayo Clinic, Jacksonville, FL, USA. ⁴⁸These authors contributed equally: Karina Cal, Alejandro Leyva.

✉ e-mail: chini.eduardo@mayo.edu; batthyany@pasteur.edu.uy; escande@pasteur.edu.uy

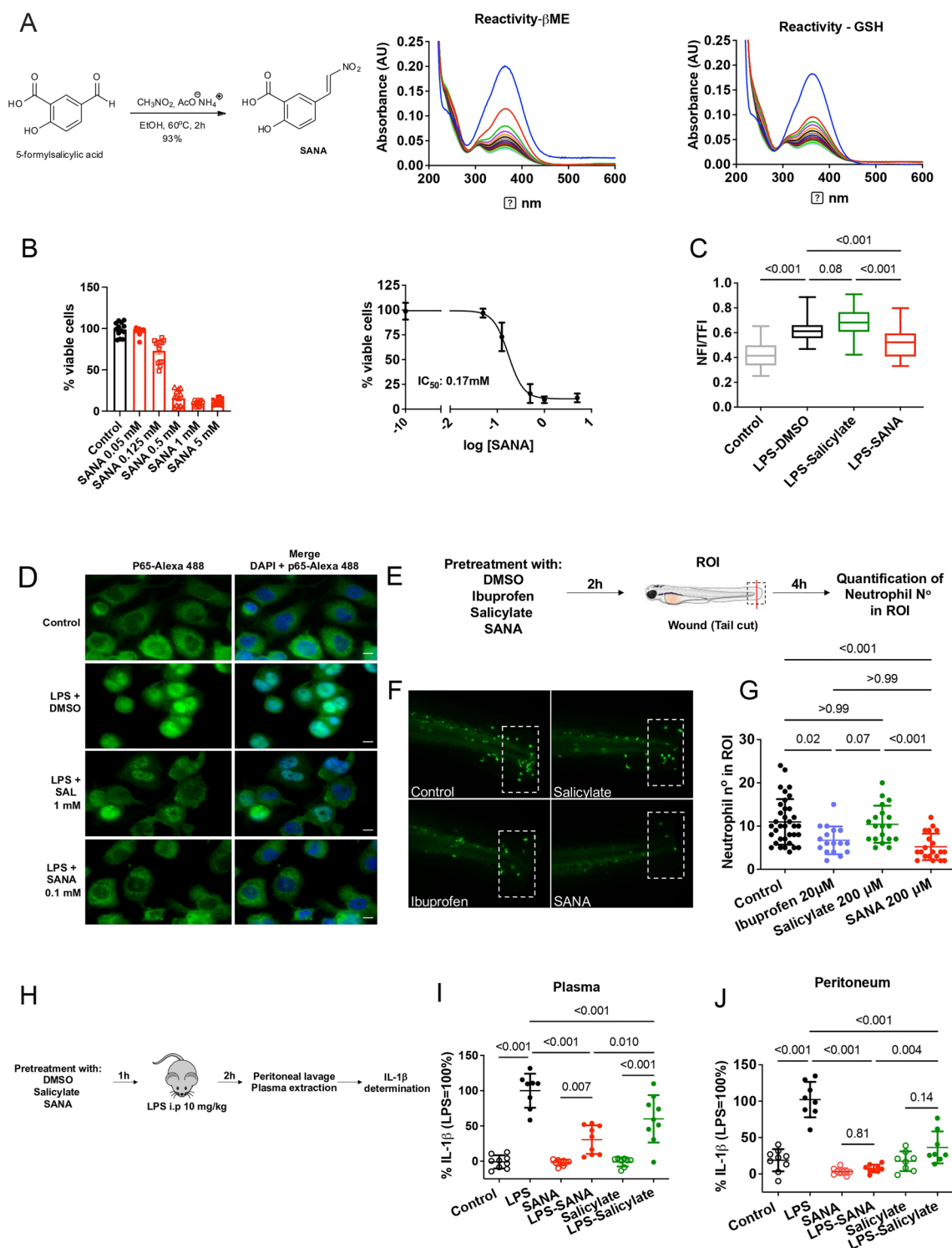
Extended Data Table 1 | Demographic Characteristics of Volunteers in SAD and MAD Studies and Baseline-to-End (Day 1 to Day 15) Treatment Profile of MAD Cohorts

Demographic and clinical characteristics of the single ascending dose (SAD) participants at baseline												
SAD GROUP	Number of patients		17		Race or ethnic group		Number (%)		Average body weight/ weight range (kg)		74 /58-102	
	Average patient age (years)		36		White		15 (88%)		Average Body Mass Index / range		25 / 20-30	
	Age range (years)		18-58		Asian		1 (6%)		BMI Distribution		Number (%)	
	Number (percent) of female patients		8 (47%)		Black		0		<20		0 (0%)	
					Other		1 (6%)		≥20 - <25		7 (41%)	
	Number (percent) of male patients		9 (53%)		Hispanic or Latino		4 (24%)		≥25 - ≤30		10 (59%)	
	Doses by Cohort				mg/dose				Doses (mg/dose/Kg) by Cohort		Average (range)	
	SAD 1				200				SAD 1		2.8 (2.7 - 3.3)	
	SAD 2				400				SAD 2		5.3 (3.3 - 6.9)	
	SAD 3				800				SAD 3		11.4 (8.3 - 13.9)	
Demographic and clinical characteristics of the multiple ascending dose (MAD) participants at baseline												
MAD GROUP	Number of patients		24		Race or Ethnic Group		Number (%)		Average body weight / weight range (kg)		93 / 77-109	
	Average patient age (years)		35		White		13 (57%)		Average body mass index		31 / 28-34	
	Age range (years)		26-55		Asian		7 (30%)		BMI distribution		Number (%)	
	Number (percentage) of female patients		5 (22%)		Black		1 (4%)		≥28 - <30		10 (43%)	
					Other		2 (9%)		≥30 - ≤35		13 (57%)	
	Number (percent) of male patients		18 (78%)		Hispanic or Latino		4 (17%)		>35		0	
	Doses by cohort				mg/dose				Doses (mg/dose/Kg) by Cohort		Average (range)	
	MAD 1				100				MAD 1		1.0 (0.9 - 1.2)	
	MAD 2				150				MAD 2		1.7 (1.4 - 1.9)	
	MAD 3				200				MAD 3		2.1 (1.9- 2.2)	
Characteristics of MAD participants in each cohort at the baseline (day 1) and at the end of the treatment (day 15)												
PLACEBO												
	Weight (kg)		BMI		Fasting Glucose (g/L)		Fasting Insulin (mU/L)		HOMA-IR		Fructasamine (umol/L)	
	day 1	day 15	day 1	day 15	day 1	day 15	day 1	day 15	day 1	day 15	day 1	day 15
Placebos	p = 0,21 (n = 3)		p = 0,24 (n = 3)		p = 0,17 (n = 5)		p = 0,19 (n = 5)		p = 0,13 (n = 5)		p = 0,48 (n = 5)	
P1	108.3	ND	33.1	ND	0.92	0.86	9	7	2.0	1.5	< 30	324
P2	82.4	ND	28.1	ND	0.86	0.83	8	9	1.7	1.8	295	303
P3	83.7	81.7	30.8	30.1	0.85	0.76	13	11	2.7	2.1	256	242
P4	103.6	103.5	34.4	34.4	0.74	0.77	7	5	1.3	1.0	263	198
P5	89.1	88.2	29.6	29.3	0.74	0.72	6	6	1.1	1.1	215	238
ACTIVE												
	Weight (kg)		BMI		Fasting Glucose (g/L)		Fasting Insulin (mU/L)		HOMA-IR		Fructasamine (umol/L)	
MAD Coh.1	day 1	day 15	day 1	day 15	day 1	day 15	day 1	day 15	day 1	day 15	day 1	day 15
200 mg/day	p = ND (n = 1)		p = ND (n = 1)		p = 0,01 (n = 5)		p = 0,10 (n = 5)		p = 0,05 (n = 5)		p = 0,22 (n = 5)	
P6	97.7	ND	30.7	ND	1.24	1.01	18	20	5.5	5.0	< 30	356
P7	101.5	ND	29.2	ND	0.92	0.76	4	4	0.9	0.8	< 30	326
P8	100.4	ND	32.5	ND	0.94	0.85	14	2	3.2	0.4	323	300
P9	90.3	ND	32.9	ND	0.90	0.83	25	14	5.6	2.9	286	274

Extended Data Table 1 (continued) | Demographic Characteristics of Volunteers in SAD and MAD Studies and Baseline-to-End (Day 1 to Day 15) Treatment Profile of MAD Cohorts

P10	104.1	101	33.8	32.8	0.94	0.81	21	7	4.9	1.4	212	ND
MAD Coh.2	day 1	day 15	day 1	day 15	day 1	day 15	day 1	day 15	day 1	day 15	day 1	day 15
300 mg/day	p = 0,01 (n = 6)		p = 0,02 (n = 6)		p = 0,47 (n = 6)		p = 0,58 (n = 6)		p = 0,65 (n = 6)		p = 0,40 (n = 6)	
P11	81.1	78.9	28.3	27.5	0.81	0.81	5	6	1.0	1.2	313	322
P12	95.7	95.1	29.4	29.2	0.85	0.83	2	14	0.4	2.9	292	264
P13	78.1	76.9	30.3	29.8	0.92	0.86	13	11	3.0	2.3	266	250
P14	77.1	75	30.4	29.6	0.85	0.79	8	9	1.7	1.8	251	249
P15	83.7	83.7	29.0	29.0	0.79	0.83	6	6	1.2	1.2	312	326
P16	109.1	107.5	34.3	33.8	0.77	0.79	8	4	1.5	0.8	184	171
MAD Coh.3	day 1	day 15	day 1	day 15	day 1	day 15	day 1	day 15	day 1	day 15	day 1	day 15
400 mg/day	p = 0,01 (n = 6)		p = 0,007 (n = 6)		p = 0,31 (n = 6)		p = 0,04 (n = 6)		p = 0,03 (n = 6)		p = 0,004 (n = 6)	
P17	92.2	90.3	29.8	29.2	0.85	1.01	2	1	0.4	0.2	340	274
P18	91	88.2	30.4	29.5	0.9	0.83	7	6	1.6	1.2	280	221
P19	94.5	89.4	28.4	26.9	0.79	0.77	5	4	1.0	0.8	259	191
P20	102.4	101.9	32.4	32.2	1.01	0.88	23	18	5.7	3.9	279	213
P21	94.1	90.6	29.1	28.0	0.92	0.85	13	6	3.0	1.3	245	225
P22	91.1	89.5	32.7	32.1	1.1	0.88	8	6	2.2	1.3	394	274

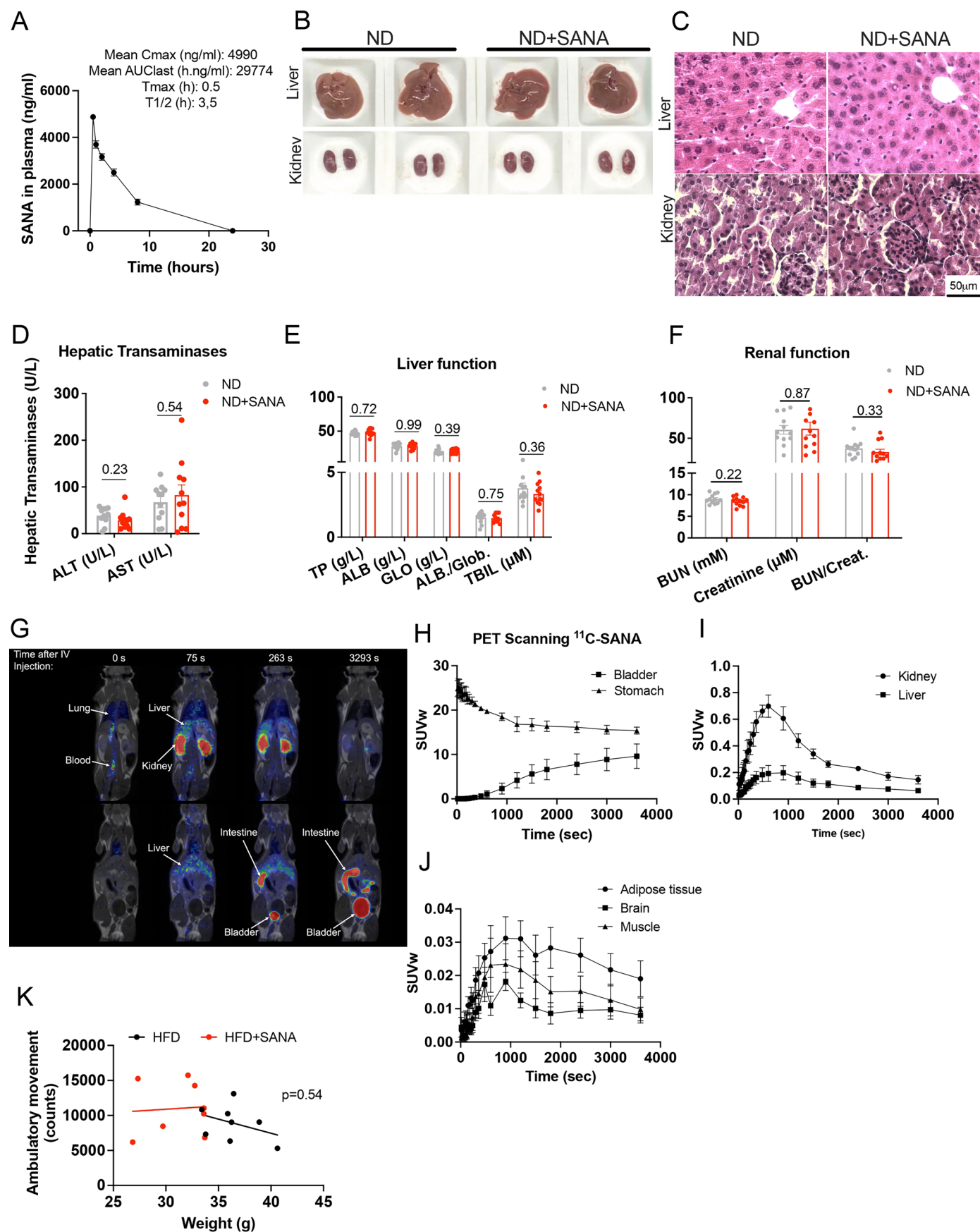
P1 to P22- ID multiple ascending dose (MAD) participants ; cohort (Coh.) of participants; ND, not determinated; P value (P) obtained performing paired t-test statistical analyses comparing day 1 vs day 15 Demographic characteristics of volunteers in SAD and MAD studies and baseline-to-end (Day 1 to Day 15) treatment profile of MAD cohorts.



Extended Data Fig. 1 | Physicochemical and biological characterization of the canonical nitroalkene effects of SANA.

(a) Synthesis (left) and electrophilic properties (right) of SANA. Spectra of SANA (10 μM) recorded every 60 s after incubation with β -Mercaptoethanol (BME, 100 μM) or reduced glutathione (GSH, 100 μM). (b) Left: cytotoxicity of SANA 24h treatment in THP-1 macrophages, measured by MTT assay. $n = 13$ per group. Right: dose-response curve fitting yielded a $\text{IC}_{50} = 0.17 \text{ mM}$, using an absorbance at 570 nm. $n = 6$ per group. (c-d) Effect of SANA on NF- κ B/p65 subunit translocation into nuclei of THP-1 macrophages. (c) Quantification of nuclear fluorescence intensity (NFI) relative to total fluorescence intensity (TFI). n : Control (DMSO) = 26; LPS-DMSO = 33; LPS-Salicylate = 56; LPS-SANA = 55. (d) Representative pictures. Cells were treated for 2 h before activation with LPS (1 $\mu\text{g}/\text{mL}$) for 30 minutes. Control: cells without LPS treatment. Bar = 10 μm . (e-g) SANA inhibition of neutrophil recruitment in

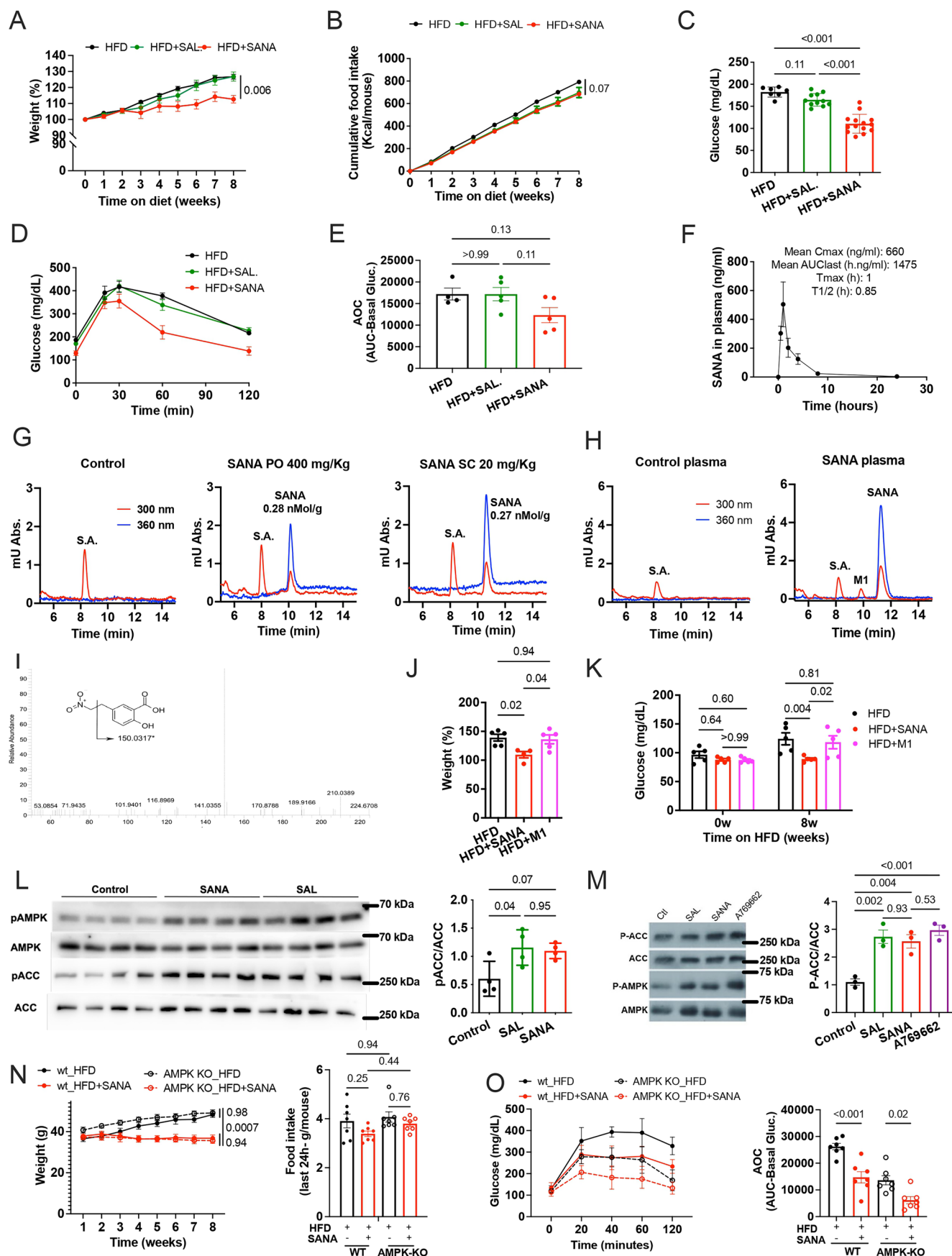
Zebrafish. (e) Acute inflammation model assay. Larvae at 3 dpf were pre-treated with DMSO, Ibuprofen, Salicylate or SANA for 2 h. Tail fins were wounded with a scalpel, larvae were maintained with the drugs and neutrophils in the injury were imaged and counted 4 h post transection. (f) Representative pictures. Dotted rectangles indicate the wounded region (ROI) where neutrophils were counted. (g) Quantification of recruited neutrophils after treatment. n : Control (DMSO) = 35; Ibuprofen 20 μM = 17; Salicylate 200 μM = 19; SANA 200 μM = 20. (h) LPS-induced inflammatory model. C57BL/6 J mice were injected IP with SANA (100 mg/kg), Salicylate (100 mg/kg) or vehicle, 1 h before IP injection of LPS (10 mg/kg) or vehicle. (i-j) ELISA quantification of IL-1 β in plasma and peritoneal lavage. n : Control = 9; LPS = 8; SANA = 9; LPS-SANA = 9; Salicylate = 8; LPS-Salicylate = 9. Data: mean \pm SEM. Statistical analyses: one-way ANOVA followed by Bonferroni post hoc for multiple comparisons (c, i, j). Kruskal-Wallis test (b).



Extended Data Fig. 2 | See next page for caption.

Extended Data Fig. 2 | Pharmacokinetics, toxicity, and tissue distribution of SANA. (a) Pharmacokinetics of SANA in mice. Mice were given a single dose of SANA (400 mg/kg) and plasma concentration was measured by LC-MS/MS over time. $n = 3$. (b–f) Toxicity effects of SANA. Mice were fed ND and administered with SANA (400 mg/kg/day, PO) for 8 weeks. (b) Liver and kidney macroscopic appearances and (c) Hematoxylin & Eosin liver and kidney staining. (d) ALT and AST in plasma/serum from mice at week 8. $n = 11$ per group. (e–f) Panel of liver (E) and renal (F) function markers (TP, ALB, GLO, TBIL and BUN). $n = 12$ per

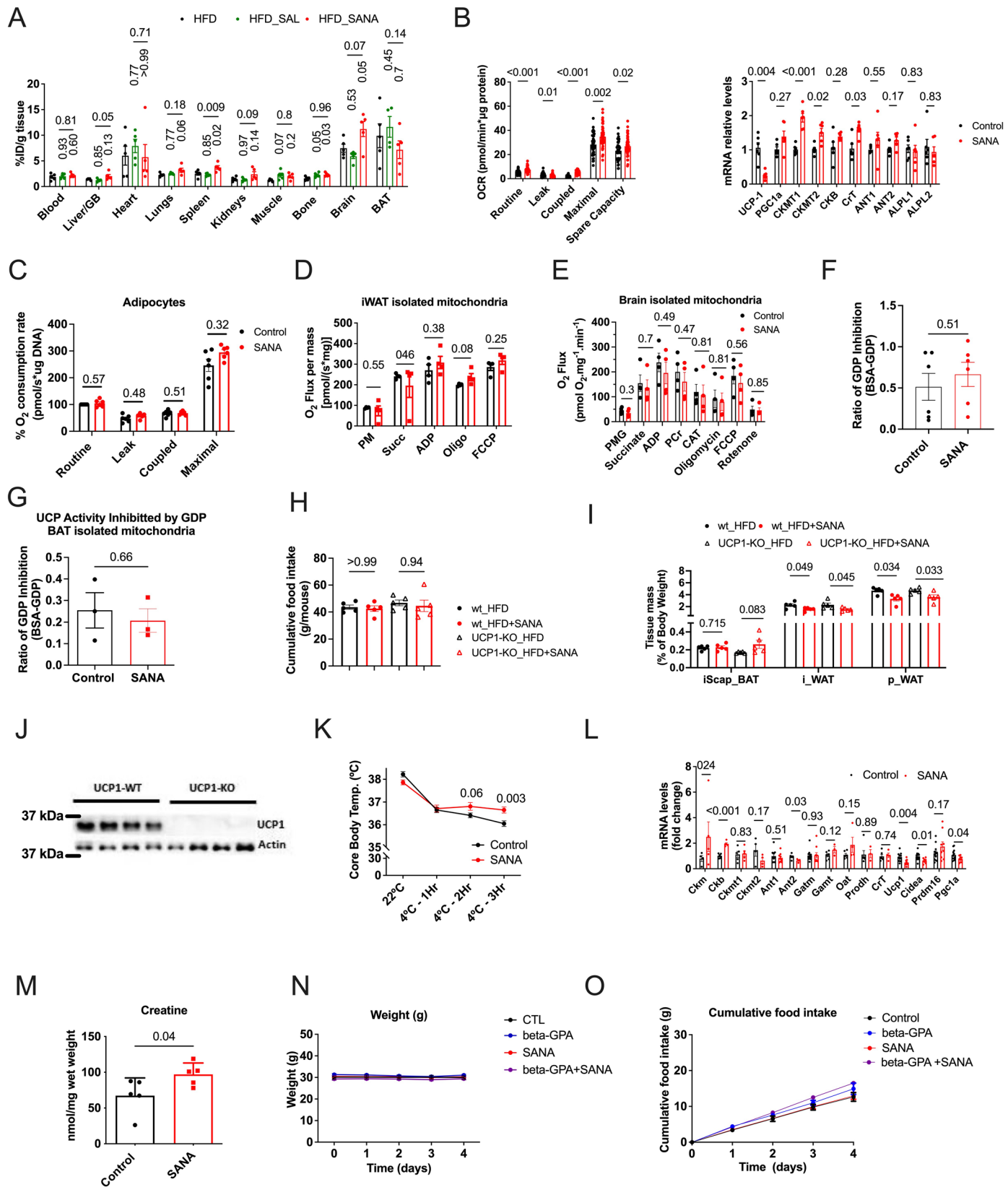
group. (g–j) Biodistribution analysis performed by IIC-SANA (9 MBq/animal) followed by PET-MRI scan. PET-scanning was performed the first 60 minutes after injection. (g) Representative picture of mice injected with IIC-SANA and followed by PET-MRI scans over time that were used to perform the analysis. (h) bladder and stomach, (i) kidney and liver, and (j) iWAT, brain, and muscle. (h–j) $n = 3$. (k) ANCOVA analysis of ambulatory activity of mice treated with HFD or HFD + SANA (400 mg/kg/day, PO) at week 8. $n = 8$ per group. Data: mean \pm SEM. Statistical analyses: unpaired two-sided Student's t -test (d, e, f). ANCOVA (k).



Extended Data Fig. 3 | See next page for caption.

Extended Data Fig. 3 | Effect of SANA formulation, main metabolite and evaluation of AMPK activation. (a–e) SANA (or SAL) were daily injected SC at 20 mg/kg. (a) Percent of weight on day 0. n = 5 per group. (b) Cumulative food intake. n = 2 per group (c) Basal glucose levels. n: HFD = 7; HFD + SAL = 11; HFD + SANA = 14. (d–e) GTT (d) and GTT AOC (e) at week 6. n: HFD = 4; HFD + SAL = 5; HFD + SANA = 5. (f) Pharmacokinetics of SANA (single dose of 20 mg/kg, SC). SANA in plasma was determined at different time points by HPLC. n = 3. (g) Representative chromatograms of steady state levels of different SANA formulations (400 mg/kg/day, PO and 20 mg/kg/day, SC) in iWAT. Salicylic acid (S.A.) was used as an internal standard. (h–i) Chromatograms of organic extraction of plasma from control mice (H left) and SANA-treated mice (H right). M1 indicates the peak assigned to SANA main metabolite 5-(2-nitroethyl)salicylic acid by MS (i). (j) Percent of initial weight (day 0) of mice fed with HFD and treated with SANA or M1 (20 mg/kg/day, SC) for 8 weeks. n: HFD = 5; HFD + M1 = 5;

HFD + SANA = 4. (k) Basal glucose levels at the onset of the experiment (0w) or after 8 weeks (8w) of HFD, HFD + SANA or HFD + M1 (20 mg/kg/day, SC). n = 5 per group. (l–m) Acute AMPK activation by SANA and SAL in vivo and in vitro. (l) Mice were treated with SANA, SAL (200 mg/kg, IP) or vehicle. AMPK activation was determined 1 h later by AMPK phosphorylation (Thr172) and ACC phosphorylation (S80) in the liver. n = 4 per group. (m) AMPK activation was measured in 3T3L1 adipocytes treated with 100 μ M of SAL or SANA. A769662 (10 μ M) was used as positive control. n = 3 per group. (n–o) Effect of SANA (20 mg/kg/day, SC) in AMPK KO (a1) mice in HFD. n = 7 per group. (n) Weight (left) and food intake (right), after 8 weeks. (o) GTT (left) and GTT AOC (right) at week 8. Data: mean \pm SEM. Statistical analyses: two-way ANOVA followed by Tukey's multiple comparisons test (a, b, k, n, o), one-way ANOVA followed by Bonferroni post hoc for multiple comparisons (c, e, j, l, m).

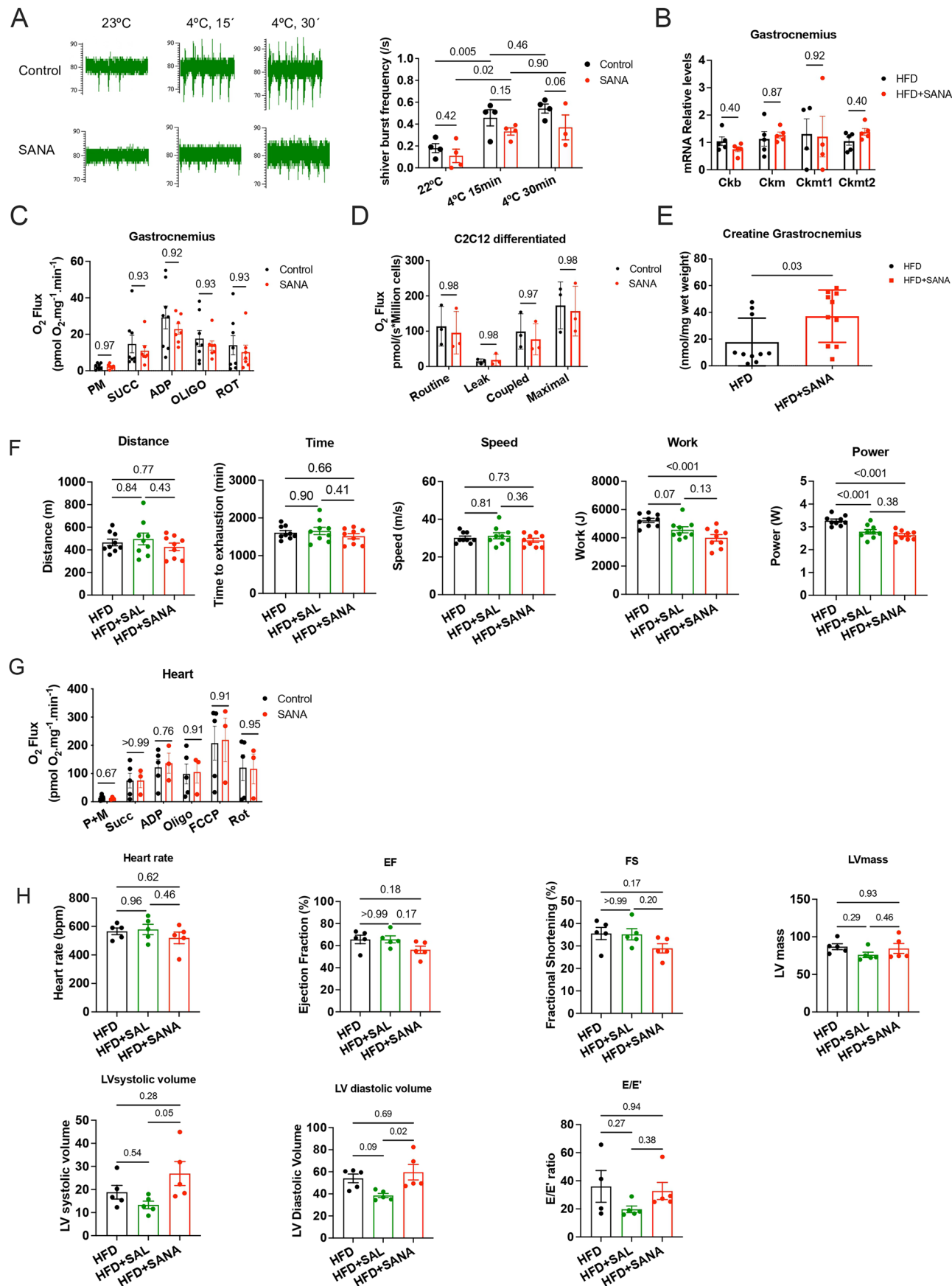


Extended Data Fig. 4 | See next page for caption.

Extended Data Fig. 4 | SANA stimulates creatine-dependent thermogenesis and promotes weight loss independently of UCP1 expression and activation.

(a) 18FDG uptake in different tissues of mice fed with HFD, HFD + SANA or HFD + SAL, 400 mg/kg/day, PO for 8 weeks. n = 5 per group. (b) Differentiated human white adipose cells (TERT-hWA) were incubated with SANA (100 μ M), for 24 hours. Left: mitochondrial respiration. n: Control=44; SANA = 48. Right: thermogenic markers measured by qRT-PCR. n = 6 per group. (c) Respiration of adipocytes isolated from mice fed with HFD for 8 weeks. Cells were incubated with SANA 100 μ M or vehicle (DMSO) n = 6 per group. (d–e) Respiration of mitochondria isolated from adipocytes (D) or brain (E), incubated with SANA (100 μ M) or vehicle. n = 4 per group. (f) Effect of GDP on respiration, calculated from data in Fig. 5f. n = 6 per group. (g) Effect GDP on UCP1 activity of isolated mitochondria from BAT, incubated with SANA (100 μ M) or vehicle. n = 3 per group. (h–i) Cumulative food intake (H) and tissue mass (I) of WT and UCP1-KO mice treated with SANA (20 mg/kg/day SC), measured at the end of treatment.

n = 5 per group. (j) UCP1 expression in BAT from WT and UCP1-KO. n = 4 per group. (k) Cold challenge. Mice were treated with SANA (20 mg/kg/day, SC) or vehicle. n = 14 per group. (l–m) Effect of SANA on cold response in mice. (L) Expression of thermogenic markers in iWAT measured by qRT-PCR after 6 hours of cold exposure. n: Supplementary Tables. (M) Creatine quantification in iWAT in mice treated as described in L. n = 5 per group. (n–o) Effect of the creatine antagonist β -GPA in mice treated with SANA previous to cold. (N) Weight gain. n: Control=15; β -GPA = 9; SANA = 16; SANA+ β -GPA = 10 and (O) cumulative food intake. n: Control=3; β -GPA = 2; SANA = 3; SANA+ β -GPA = 2. Data: mean \pm SEM. Statistical analyses: one-way ANOVA followed by Bonferroni post hoc for multiple comparisons (A); two-way ANOVA followed by Tukey's multiple comparisons test (H, I, K); unpaired two-sided Student's t-test (B–G, L–M). Vertical p-values indicate multiple comparisons of each experimental condition vs the control condition (HFD in A).

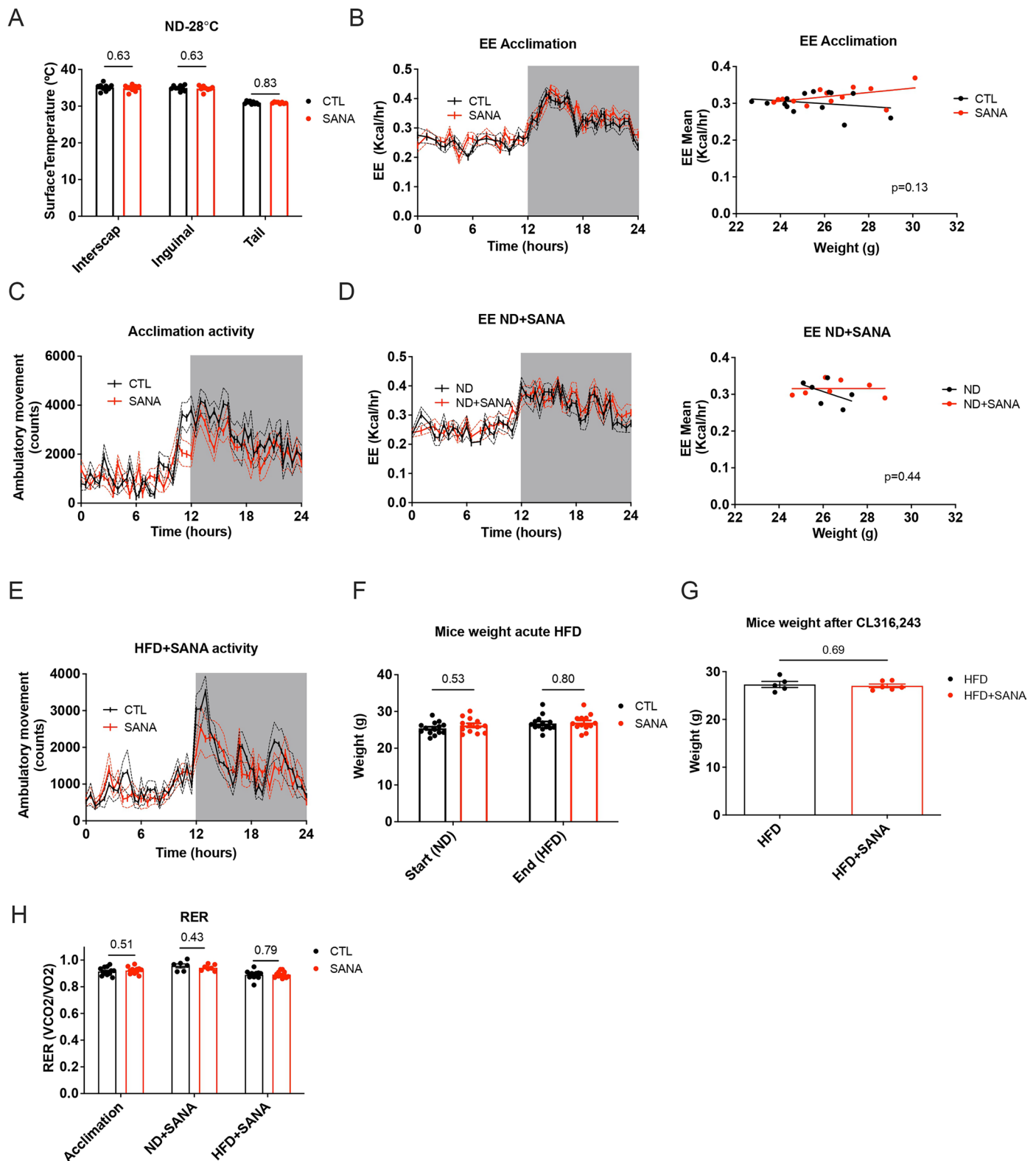


Extended Data Fig. 5 | See next page for caption.

Extended Data Fig. 5 | Effect of SANA on skeletal and cardiac muscle function.

(a) Electromyogram at 15 and 30 min time points during cold exposure of mice treated daily with SANA (20 mg/kg/day, SC) or vehicle for 5 consecutive days before cold exposure. n = 4 per group. (b) qRT-PCR analysis of creatine kinases expression in gastrocnemius muscle. n: n = 5 for Ckb, Ckm and Ckmt2; n = 4 for Ckmt1 (c) Respiration of gastrocnemius permeabilized fibers from mice treated or not with SANA (20 mg/Kg/day, SC), and after addition of substrates (PM: pyruvate-malate; SUCC: succinate; ADP) and inhibitors (OLIGO: oligomycin and ROT: rotenone). n: Control=8; SANA = 7. (d) Assessment of mitochondrial respiration in differentiated C2C12 myoblasts n = 3 per group. (e) Creatine levels

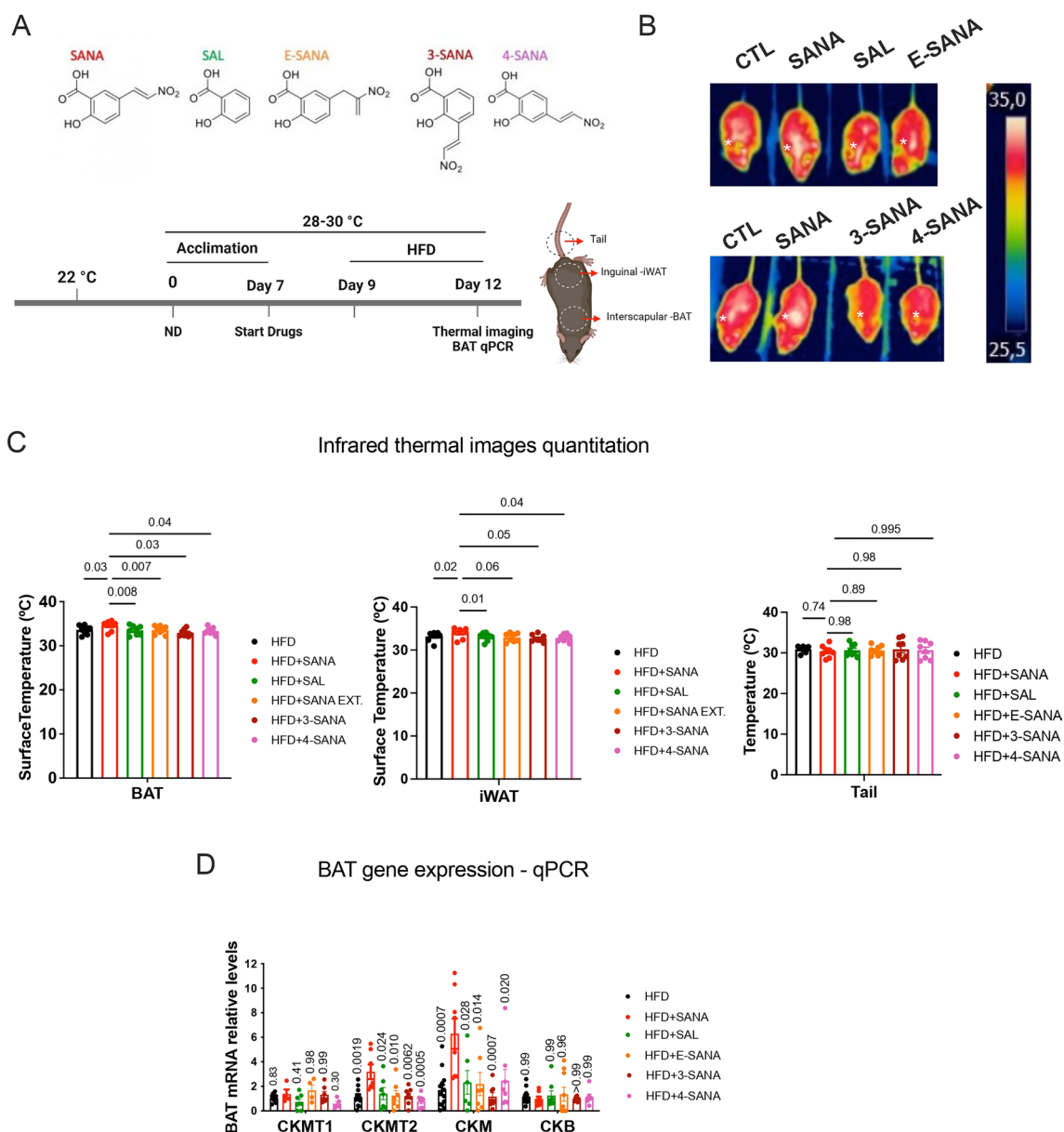
measured by NMR of mice treated with HFD or HFD + SANA (400 mg/kg/day, PO). n = 10 per group. (f) Aerobic muscle capacity measured in the treadmill at the end of treatment. Mice were fed during 22 weeks with HFD and HFD + SANA (or SAL) at 400 mg/kg/day, PO. n = 9 per group. (g) Respiration of permeabilized fibers from heart muscle from mice treated with SANA (20 mg/kg/day, SC). n: Control=5; SANA = 3. (h) Echo Cardiac function assessment in mice in HFD or HFD + SANA (or SAL) at 400 mg/kg/day, PO after 22 weeks of treatment. n = 5 per group. Data: mean \pm SEM. Statistical analyses: one-way ANOVA followed by Bonferroni post hoc for multiple comparisons (f, h); two-way ANOVA followed by Tukey's multiple comparisons test (a); unpaired two-sided Student's t-test (b, c, d, e, g).



Extended Data Fig. 6 | Supporting additional information to CLAMS data of mice under acute HFD and SANA treatment under thermoneutral conditions.

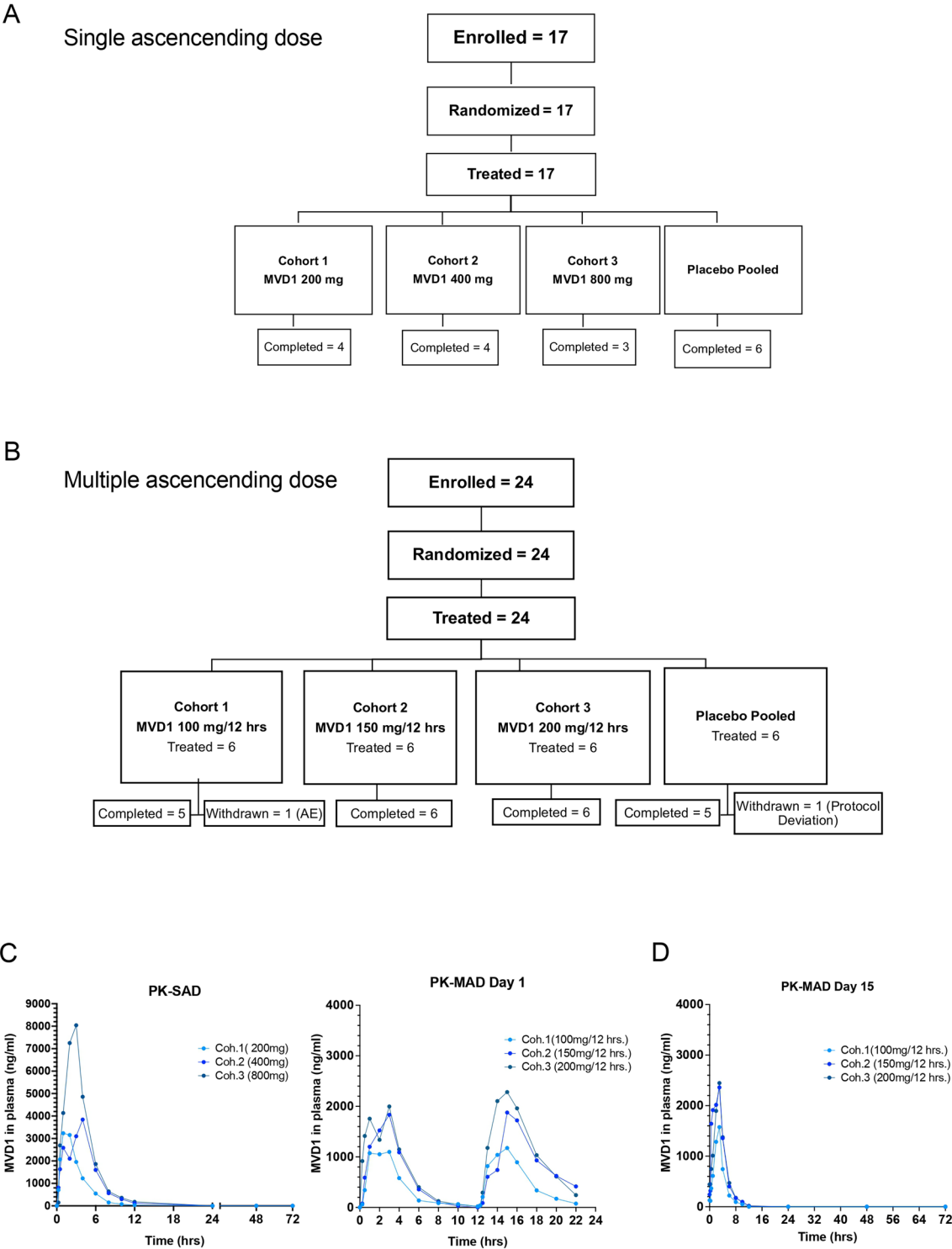
(a) Surface temperature quantification from thermal images of mice fed with ND and treated with SANA under thermoneutral conditions (day 9). $n=9$ per condition. (b) Left: EE measurements over a 24-hour period at the end of the acclimation period at thermoneutrality (day 7). Right: regression plot of these data. n : CTL = 14; SANA = 13. (c) Total activity over a 24-hour period during acclimation (day 7). n : CTL = 14; SANA = 13 (d) Left: EE Measurements over a 24-hour period at the end of SANA treatment under ND feeding (day 9). Right: regression plot of these data. n : CTL = 6; SANA = 7 (e) Total activity over a 24 h

period at the end of SANA treatment under HFD. n : CTL = 14; SANA = 13. (f) Mice weight at the beginning and end of the acute HFD treatment. n : CTL = 14; SANA = 13. (g) Mice weight after acute single treatment with CL316,243 (1 mg/kg). n : HFD = 5; HFD + SANA = 6. (h) Respiratory exchange ratio (RER) from mice under acute HFD treatment at the end of acclimation period (day 7), at the end of ND + SANA (day 9) and at the end of HFD + SANA (day 12). n : CTL = 14; SANA = 13. Data: mean \pm SEM. Statistical analyses: paired two-sided Student's t -test (A), unpaired two-sided Student's t -test (G, H), two-way ANOVA followed by Tukey's multiple comparisons test (f), ANCOVA (b, d).



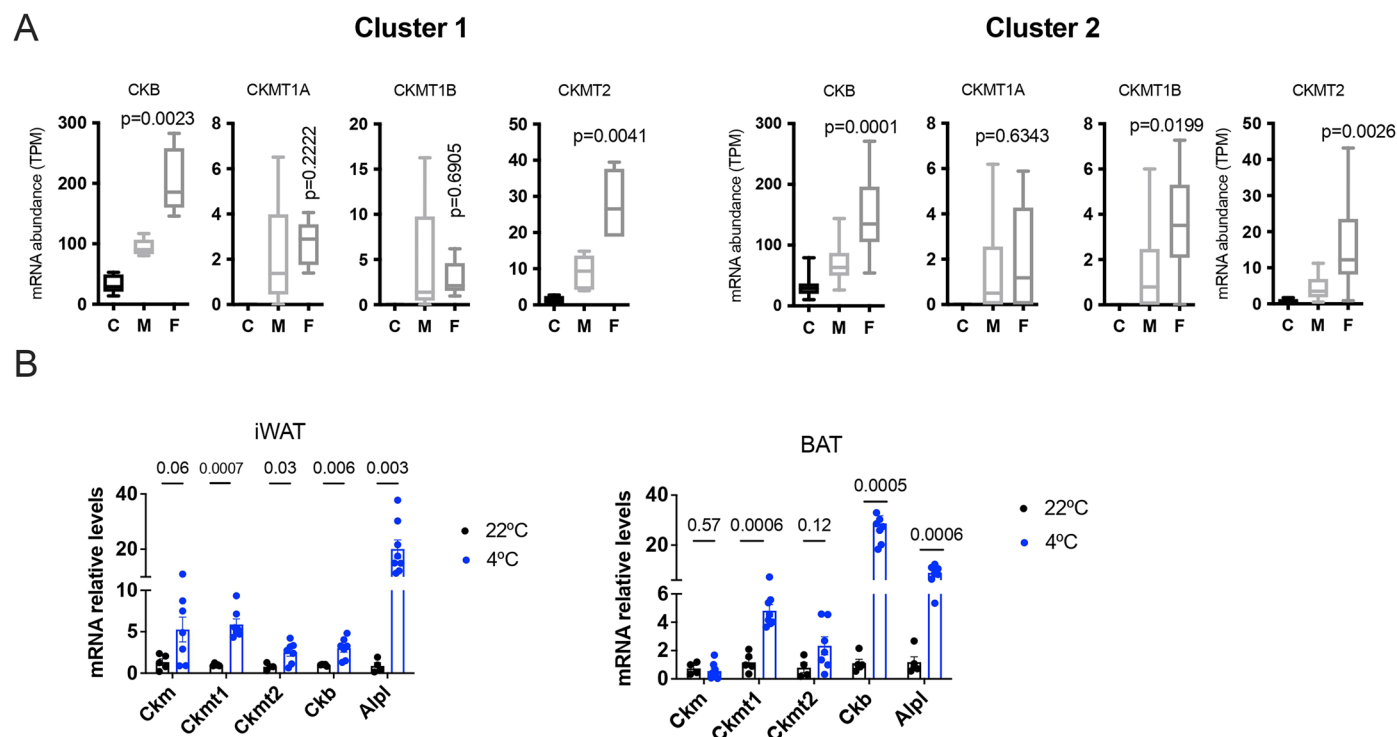
Extended Data Fig. 7 | Effect of SANA isomers (3-SANA, 4-SANA) and analog (E-SANA) on creatine induced thermogenesis. (a) Chemical structure of synthesized and tested analogs and experimental strategy to evaluate their effect on thermogenesis. Mice were treated with different compounds (20 mg/kg/day, SC) following the same protocol described in Fig. 6f (acute HFD). Created with [BioRender.com](https://www.biorender.com). (b) Representative thermal images. (c) Quantitation of thermal

images corresponding to BAT, iWAT and tail regions at the end of the treatment. $n = 8$ per group. (d) qRT-PCR analysis of creatine kinases in BAT at the end of the treatment. n : Supplementary Tables. Data: mean \pm SEM. Statistical analyses: One way ANOVA followed by Bonferroni post hoc for multiple comparisons (c, d). Expressed p-values indicate multiple comparisons of each experimental condition vs the condition of mice treated with SANA (HFD + SANA in c and d).



Extended Data Fig. 8 | Extended clinical information. (a-b) Clinical trial design for Single Ascending Dose (SAD) (a) and Multiple Ascending Dose (MAD) (b). (c) Pharmacokinetics of MVD1 in SAD and MAD, Day 1. The calculation of the pharmacokinetics parameters is presented in Supplementary Tables. (d)

Pharmacokinetics of the last dosage given to volunteers from MAD at day 15 of administration. The calculation of the pharmacokinetics parameters is presented in Supplementary Tables.



Extended Data Fig. 9 | Gene expression of creatine kinases during different thermogenic stimuli. (a) RNAseq expression analysis of all creatine kinases in two clusters of human adipocytes progenitor cells (10.1073/pnas.1906512116). Respective statistical comparisons were set between vehicle-treated differentiated adipocytes (M), and forskolin-treated differentiated adipocytes (F). C corresponds to adipocytes maintained in a non-differentiated state. $n = 5$ per group in cluster 1-lipogenic adipocytes (Left) and $n = 14$ per group in cluster 2-thermogenic adipocytes (right). CKM was not present in the public dataset

analyzed. **(b)** Analysis of creatine kinases and the Alpl phosphatase expression by qRT-PCR in iWAT and BAT from mice fed with ND and maintained at room temperature (22 °C) or after a prolonged cold challenge (48 hours at 4 °C). iWAT: 22 °C $n = 5$ for Ckm, Ckmt1 and Ckb; $n = 4$ for Ckmt2 and Alpl; 4 °C $n = 7$ for Ckm, Ckmt1, Ckmt2 and Ckb; $n = 8$ for Alpl. BAT: 22 °C $n = 4$ for Ckm and Ckmt2; $n = 5$ for Ckmt1, Ckb and Alpl; 4 °C $n = 8$ for Ckm, Ckmt1, Ckb and Alpl; $n = 7$ for Ckmt2. Data: mean \pm SEM. Statistical analyses: unpaired two-sided Student's t-test **(a,b)**.